Geochemistry, Geophysics, Geosystems®

RESEARCH ARTICLE
10.1029/2023GC011161

Mobilization of Tungsten in Greenstone Belts of the Archean Kaapvaal and Singhbhum Cratons

N. Messling[1], J. Jodder[2,3], E. Hegner[4], A. Hofmann[5], K. Wemmer[1], and M. Willbold[1]

[1]Department for Geochemistry and Isotope Geology, Georg-August-Universität Göttingen, Göttingen, Germany, [2]Evolutionary Studies Institute, University of the Witwatersrand, Johannesburg, South Africa, [3]Centre for Planetary Habitability (PHAB), University of Oslo, Oslo, Norway, [4]Department of Earth and Environmental Sciences & GeoBio-Center, Ludwig-Maximilians-Universität, München, Germany, [5]Department of Geology, University of Johannesburg, Johannesburg, South Africa

Key Points:

- The magmatic sources of metavolcanic rocks from the Onverwacht Group and the Badampahar Group do not exhibit W isotope anomalies
- Negative W isotope signatures in the Onverwacht Group are likely derived from fluids sourced from younger intrusive granitoids
- Felsic intrusive rocks are a major source of W-rich fluids in Paleoarchean greenstone units

Supporting Information:

Supporting Information may be found in the online version of this article.

Correspondence to:

N. Messling,
nils.messling@uni-goettingen.de

Citation:

Messling, N., Jodder, J., Hegner, E., Hofmann, A., Wemmer, K., & Willbold, M. (2023). Mobilization of Tungsten in Greenstone Belts of the Archean Kaapvaal and Singhbhum Cratons. *Geochemistry, Geophysics, Geosystems*, *24*, e2023GC011161. https://doi.org/10.1029/2023GC011161

Received 31 JUL 2023
Accepted 22 NOV 2023

Abstract Due to the inherently fluid-mobile nature of W, the ^{182}W record of the early Earth may have been obscured by fluid-induced mobilization of W. To investigate W mobilization in Archean greenstone sequences, we analyzed ^{182}W isotope systematics and major and trace element concentrations in samples from the 3.53 Ga old Onverwacht Group of the Kaapvaal Craton (South Africa) and the >3.51 Ga old Badampahar Group of the Singhbhum Craton (India). Our results for mafic and ultramafic metavolcanic rocks show W/Th ratios significantly higher than primary magmatic values, which suggests fluid-induced W enrichment. Samples least affected by secondary W enrichment (W/Th < 0.26) show no resolvable W isotope anomalies from modern mantle values in both cratons. Samples from the Kaapvaal Craton with elevated W/Th exhibit deficits in ^{182}W as low as -8.1 ± 4.3 ppm compared to the modern mantle. Covariations of μ^{182}W with W/Th, and Ce/Pb suggest that negative isotope signatures were introduced during secondary fluid-mediated processes. The enrichment of W is most evident in altered ultramafic rocks comprising serpentine, resulting in additional covariations between MgO, LOI, and W/Th. The W isotope composition of serpentinized komatiites reflects the composition of younger intruding granitoids. We therefore infer the latter as a possible source of W-rich fluids. The Badampahar Group samples exhibit little W isotope variability. A well-resolved ^{182}W deficit of -6.2 ± 2.9 ppm was determined in a single komatiite sample, which indicates an unknown fluid source, currently not represented in any other unit of the Singhbhum Craton.

Plain Language Summary The tungsten (W) isotope composition of ancient rocks can be used to trace processes that occurred during Earth's early evolution. However, interactions between rocks and fluids may alter the W concentration and therefore influence the interpretation of W isotope data. To identify the source of such fluids and the processes by which they affect the W isotope composition of rocks, we analyzed ancient rock samples from South Africa and India. The isotope composition of rocks with a low W concentration reflects that of the modern Earth. Therefore, they do not trace the processes that occurred during Earth's early evolution. Samples from South Africa with untypically high W concentrations show a different isotopic composition. The variation in the W isotope signature correlates with other chemical indices that are susceptible to modification by fluid-related processes. This shows that the W within the rocks is derived from an external fluid source and not from their original magmatic source. Samples with the highest W enrichment have a similar isotope composition as spatially associated intrusive rocks. By inference, the latter likely represent the source of W-rich fluids. The samples from India show similar enrichment in W, indicating similar fluid-related processes and W sources at both localities.

1. Introduction

Although geological evidence of Earth's oldest continental crust is poorly preserved due to its continued destruction through plate tectonic processes over billions of years, rare occurrences of early crust in Archean cratonic nuclei offer a unique opportunity to investigate Earth's earliest geological history. Extinct radiogenic isotope systems, like the ^{182}Hf-^{182}W (half-life of 8.9 Myr; Vockenhuber et al., 2004) can provide valuable information on Earth's accretion, planetary-scale differentiation, and mantle evolution. Excesses in the ^{182}W/^{184}W ratio relative to those observed in the modern upper mantle have been previously reported in Archean rocks. They have been interpreted in the context of protracted terrestrial accretion in a "late veneer" scenario (e.g., Archer et al., 2019; Dale et al., 2017; Tusch et al., 2021; Willbold et al., 2011, 2015) as well as silicate differentiation in an early

magma ocean (e.g., Puchtel et al., 2016; Rizo et al., 2016; Touboul et al., 2012, 2014). Building upon these studies, models describing the local and global evolution of W isotope heterogeneities in the Archean mantle through time were formulated, aiming at a better understanding of the geodynamic conditions of the Archean Earth (Nakanishi et al., 2023; Puchtel et al., 2022; Tusch et al., 2021). Crucially, this goal requires that the observed W isotope composition of metavolcanic Archean rocks represents the composition of their mantle sources. However, all Archean cratons have been affected by multiple and very often pervasive metamorphic and metasomatic events. These range from seafloor alteration (carbonatization, silicification, serpentinization), regional greenschist to amphibolite facies metamorphism, contact metamorphism during plutonic intrusion to modern surface weathering (e.g., Diener et al., 2005; Dziggel et al., 2002; Hofmann & Harris, 2008; Lécuyer et al., 1994; Nakamura & Kato, 2004; Shibuya et al., 2010). This has important bearings on the W isotope data in these rocks and the resulting conclusions on source processes because of the inherently fluid-mobile nature of W (Bali et al., 2012; König et al., 2008; Reifenröther et al., 2021; Schmidt et al., 2020). Mobilization of W and its isotopes has been frequently recognized in a variety of Archean cratons (Rizo et al., 2016; Tusch et al., 2021; Willbold et al., 2015). Within these cratons, units affected by widespread W mobilization frequently share a similar isotopic composition, regardless of lithology, magmatic source, or age (Liu et al., 2016; Tusch et al., 2019, 2021). However, the sources of these fluids and the processes by which they affect the W budget of Archean volcanic rocks as well as the impact on the preservation of primary W isotope signatures remain poorly constrained to date (Liu et al., 2016, 2018).

In the Kaapvaal Craton, negative $\mu^{182}W$ values have been reported for the 3.42–3.55 Ga old rocks of the Barberton Greenstone-Granitoid Terrane (BGGT) and the Ancient Gneiss Complex. At present, these are the only deficits observed in $\mu^{182}W$ for Archean mantle-derived rocks and were interpreted in the context of complex multistage silicate differentiation processes during the Hadean (Puchtel et al., 2016; Tusch et al., 2022). However, the same rocks also exhibit distinct relative enrichment in W, far exceeding their assumed magmatic W budget (Puchtel et al., 2016). In the Singhbhum Craton, similar enrichment in W concentrations has been reported for 3.34 Ga old komatiites from the Gorumahisani Greenstone Belt (Chaudhuri et al., 2017). The W isotope compositions of the volcanic rocks of this craton have yet to be determined. The coeval geological evolution of these two cratons and chemical similarities in their lithologies (e.g., Hofmann et al., 2022) presents an ideal opportunity to identify possible sources of W-rich fluids in Archean cratons and gain an understanding of their influence on the W budget of volcanic rocks.

2. Geological Setting

2.1. The Barberton Greenstone-Granitoid Terrane of the Kaapvaal Craton

The 3.55–3.20 Ga Barberton Greenstone-Granitoid Terrane (BGGT) is located in the eastern part of the Kaapvaal Craton in South Africa (Figure 1a). Therein the tightly folded sedimentary and volcanic strata of the Barberton Supergroup are preserved. The latter is divided into the lowermost Onverwacht Group comprising predominantly sub-marine basaltic and komatiitic volcanic rocks interlayered with subordinate felsic volcanic rocks and the largely sedimentary Fig Tree and Moodies groups (de Wit et al., 2011; Viljoen & Viljoen, 1969). The structurally lowermost unit of the Onverwacht Group comprises the Sandspruit and Theespruit formations. The Sandspruit Formation mostly comprises pillowed basalts and strongly sheared mafic-ultramafic schists. Besides locally pillowed basalts, felsic volcanic and volcaniclastic rocks frequently occur in the Theespruit Formation (de Wit et al., 1987; van Kranendonk et al., 2009). Both units were emplaced contemporaneously at around 3.55–3.53 Ga and therefore likely represent a single lithostratigraphic unit (Kröner et al., 2013, 2016). Notably, the Sandspruit Formation occurs as rafts and slivers surrounded by tonalites and trondhjemities of the 3.45 Ga Stolzburg and Theespruit plutons as well as a variety of smaller plutonic intrusions forming a coherent crustal block, referred to as the Stolzburg Block (Figure 1a; Moyen et al., 2019). The Steynsdorp tonalite pluton in the southeastern part of the BGGT is mantled by the Sandspruit and Theespruit formations. With an age of 3.51 Ga (Kröner et al., 1996), the Steynsdorp Pluton represents the oldest TTG intrusion of the BGGT followed by the granitoids of the Stolzburg Block. Within the Stolzburg Block, a trail of greenstone fragments has been interpreted as equivalents of the Sandspruit and Theespruit formations (Anhaeusser, 2014). The largest of these greenstone fragments is the Schapenburg Greenstone Remnant (SGR), which consists of cyclical layered volcano-sedimentary sequences, comprising massive komatiite flows (Anhaeusser, 2014). A whole-rock ^{187}Re-^{187}Os isochron on SGR komatiites yielded an age of 3,549 ± 99 Ma, which is consistent with that of the lower Onverwacht Group (Puchtel et al., 2009). The lower Theespruit Formation is separated from the komatiite sequences of the 3.48 Ga Komati

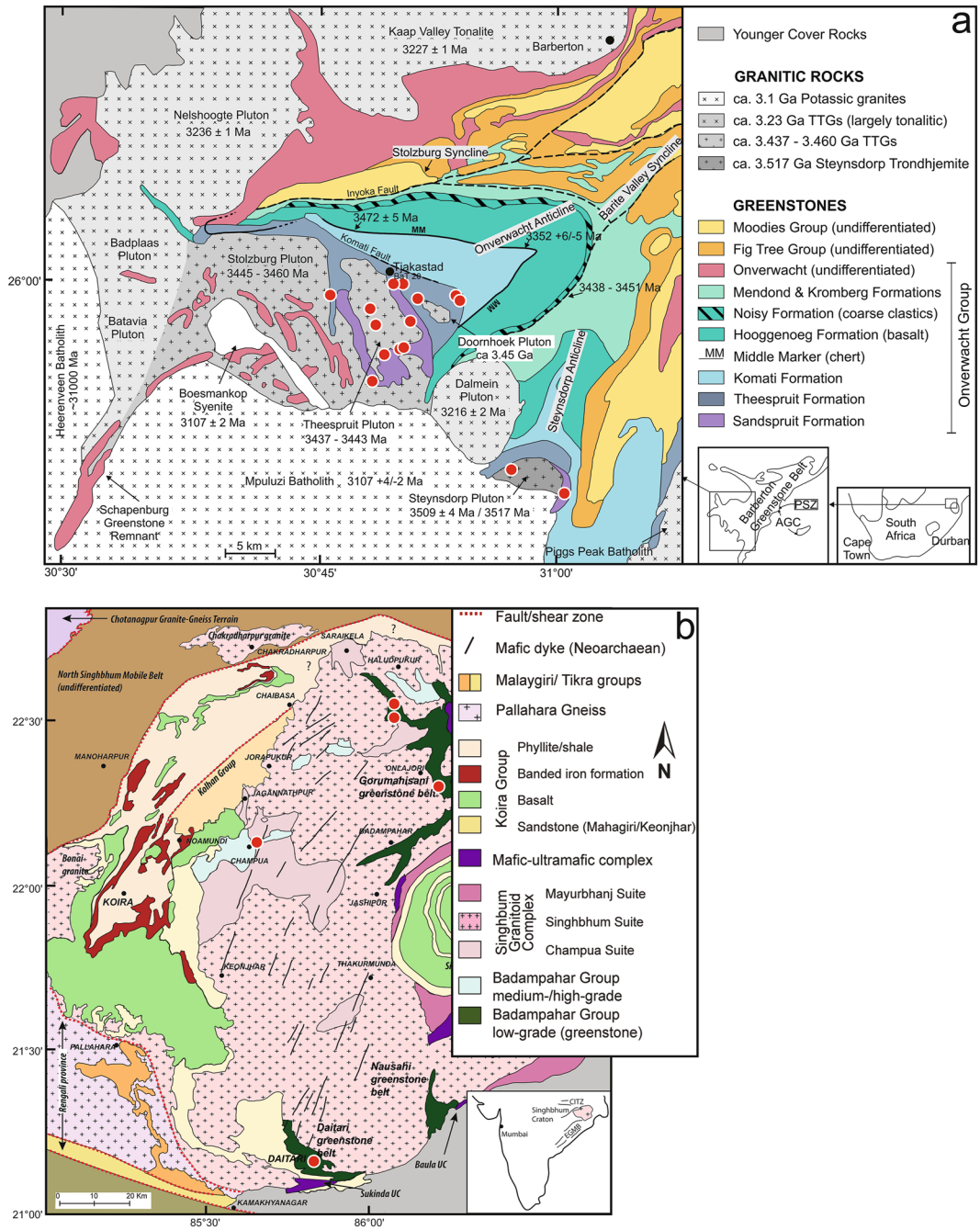

Figure 1. (a) Geological map of the BGGT modified after Schneider et al. (2019) and Grosch et al. (2011). (b) Geological map of the Singhbhum Craton modified after Hofmann et al. (2022). All sample locations are marked with red dots. The coordinates for the sample locations are provided in Data set S1 of the Supporting Information S1.

Formation by a ductile shear zone known as the Komati Fault, which separates the mostly lower greenschist-facies assemblages of the Komati Formation from the amphibolite-facies Sandspruit and Theespruit formations (van Kranendonk et al., 2009).

2.2. The Daitari and Gorumahisani Greenstone Belts of the Singhbhum Craton

The Paleoarchean Daitari and Gorumahisani greenstone belts are situated near the southern and northern margins of the Singhbhum Craton, respectively, and were assigned to the Badampahar Group (Figure 1b; Hofmann

et al., 2022; Jodder et al., 2023). The Daitari Greenstone Belt comprises mafic and ultramafic rocks as well as minor chemical sedimentary and felsic volcanic rocks and has been subdivided into five major lithostratigraphic formations (Jodder et al., 2023). The lowermost stratigraphic unit is the >3.51 Ga old Kalisagar Formation comprising sub-marine mafic to ultramafic volcanic succession (ca. 3 km thick) with minor interbedded cherts. The Kalisagar Formation is in sharp contact with the overlying 3.51 Ga old Talpada Formation (ca. 1.5 km thick), which mostly consists of dacitic to rhyodacitic rocks with minor interbedded cherts. The Talpada Formation is overlain by the sedimentary Sindurimundi and Tomka formations. The uppermost stratigraphic unit exposed in the Daitari belt is the Talangi Formation, which is in an unconformable contact relationship with the overlying Mesoarchean siliciclastic rocks of the Mahagiri Formation. The Talangi Formation is a ca. 1 km thick suite of pillowed and massive basalts, spinifex-textured komatiitic basalts and thin interlayered cherts. Geochronological data for the emplacement of the Tomka and Talangi formations are lacking, but deposition must have taken place prior to the regional deformation at ca. 3.3 Ga (Hofmann et al., 2022). A detailed stratigraphic investigation of the Gorumahisani Greenstone Belt in the northern Singhbhum Craton, has so far not been conducted. However, a minimum age of ca. 3.51 Ga for the greenstones exposed in the Gorumahisani area has been obtained by LA-ICP-MS U-Pb dating of zircon from felsic volcaniclastic rocks (Jodder et al., 2021). The Daitari and Gorumahisani greenstone belts are both interleaved by granitoid suites of the Singhbhum Granitoid Complex. Their ages coincide with the evolution of the greenstone belts from 3.53 to <3.0 Ga (Acharyya et al., 2010; Hofmann et al., 2022; Mitra et al., 2022; Nelson et al., 2014; Olierook et al., 2019). The oldest intrusions of 3.53–3.38 Ga represent the early trondhjemite-tonalite gneisses of the Champua Suite (Hofmann et al., 2022; Mitra et al., 2022). The younger Singhbhum Suite consists of both potassic and sodic plutonic rocks dated at 3.37–3.28 Ga, whereas ∼3.1 Ga intrusive rocks of the Mayurbhanj Suite are predominantly potassic in composition (Dey et al., 2017; Hofmann et al., 2022). The Gorumahisani Greenstone Belt is surrounded by younger plutonic rocks of the Singhbhum Granitoid Complex ranging in age from 3.53 to 3.08 Ga, while intrusive rocks are dated between 3.28 and 3.01 Ga (Acharyya et al., 2010; Jodder et al., 2021; Nelson et al., 2014). The Daitari Greenstone Belt is intruded by the 3.38–3.35 Ga old Singhbhum Suite that occurs as trondhjemitic sills within the greenstones and massive granitoid intrusions at the base of the Kalisagar Formation (Figure 1b; Jodder et al., 2023).

3. Samples and Methods

The samples from the BGGT were collected from the lower Onverwacht Group. They include eight mafic to ultramafic volcanic rocks from the Sandspruit Formation and additional four basalts and 10 felsic volcanic rock samples from the Theespruit Formation (Figure 1a). Two tonalite samples from the 3.51 Ga old Steynsdorp Pluton and the 3.45 Ga old Theespruit Pluton were additionally analyzed. From the Singhbhum Craton, we analyzed >3.51 Ga mafic and felsic samples from the Gorumahisani and the Daitari Greenstone Belt (Badampahar Group). Samples from the Daitari Greenstone Belt were originally described in Jodder (2021). This study reported petrography, bulk major and trace elements for samples DM 12–97. We additionally analyzed five komatiitic basalts from the 3.3 Ga Talangi Formation (DM 301–302). From the Gorumahisani Greenstone Belt, 10 mafic to ultramafic volcanic rock samples were analyzed (HP1-4, GUD 10–14 and SB 12–14). Complementary to the volcanic rocks we analyzed a 3.37 Ga old trondhjemitic sill from the Singhbhum Granitoid Complex intrusive into the Kalisagar Formation and a granodioiritic gneiss from the Champua Suite dated at 3.45 Ga (cf. Hofmann et al., 2022). For W isotope analysis, powders were prepared from whole rock samples or crushed rock chips. Samples from the Onverwacht Group were crushed into 2–4 cm-sized pieces using a metal jaw crusher. To avoid metal contamination all pieces were washed repeatedly with high-purity water (18.2 MΩ*cm; Merck Milli-Q) to remove any dust containing metal abrasion. Fist-size samples from the Singhbhum Craton and the TTGs from the Kaapvaal Craton were cut into 1.5 cm thick slices from which all saw marks were removed with SiC grinding paper on a rotating polishing disk. All samples were then crushed to <5 mm-sized gravel using a hydraulic press. To avoid sample contact with the steel plates of the hydraulic press, the samples were wrapped in plastic bags. The rock gravel was milled using an agate ball mill, which was cleaned after each sample with high-purity quartz sand (Merck, Analytical Grade). Wet-chemical sample preparation was carried out in class 100 fume hoods housed in a metal-free, class 10,000 clean room environment. The samples were processed with double-distilled HCl, HNO_3, and HF prepared by sub-boiling distillation (Savillex DST-1000). The distilled acids were diluted with high-purity water (18.2 MΩ.cm; Merck Milli-Q) to the desired molarities for sample dissolution and chromatography. Additional method details containing major and trace analysis procedures and X-ray diffractometry analysis are provided in Text S1 of the Supporting Information S1. Major and trace element data

as well as $\mu^{182}W$ values are reported in Data set S1 of the Supporting Information S1. This includes Nd isotope data for samples from the BGGT.

3.1. Nd Isotope Analysis

The Nd isotope analyses were carried out on a ThermoFisher Scientific Neptune Plus MC-ICPMS at Göttingen University. Up to 400 mg of finely ground sample powder (equivalent to ~300 ng Nd) were weighted into pre-cleaned 15 mL screw top Savillex PFA beakers and spiked with a ^{150}Nd-^{149}Sm tracer solution. The sample powders were then digested in a mixture of 2 mL conc. HNO_3 and 2 mL conc. HF on a hotplate at 120°C for 72 hr and heated at 80°C to incipient dryness. The sample cake was dissolved in 10 mL of 6 M HCl and heated at 110°C overnight for complete sample dissolution. When necessary, this step was repeated until a clear solution was obtained. Quantitative isolation of Nd and Sm from the sample matrix generally followed the method described by Richard et al. (1976). The light rare-earth elements (LREE) were separated using quartz glass columns with a bed of 5 mL BioRad AG50x8 (200–400 mesh) resin (Richard et al., 1976). The secondary quartz glass columns for Nd and Sm separation were packed with 2 mL Triskem LN-spec resin (100–150 µm). The element fractions were dried down and subsequently diluted in 0.5 M HNO_3 to a nominal concentration of samples and reference materials of 100 ng/mL for mass spectrometry. The isotope ratios were determined on a ThermoFisher Scientific Neptune Plus MC-ICPMS equipped with nine Faraday cups. The ion currents of Nd and Sm isotopes were measured using 10^{11} Ω amplifiers and the interfering isotope monitors (i.e., ^{140}Ce and ^{149}Sm for Nd isotopes, ^{145}Nd and ^{155}Gd for Sm isotopes) were measured using 10^{12} Ω amplifiers. Sample solutions were introduced into the plasma source via a Cetac Aridus3 desolvation system and the plasma source was equipped with a standard Ni sampler and H-type skimmer cones. The determination of Nd isotope ratios are based on 100 mass scans per sample and those of Sm on 40 mass scans using a static ion-collection mode. Measurements of blank solutions (0.5 M HNO_3; 40 scans) preceded and followed those of sample solutions and reference materials. Data reduction was performed offline using a Python script for Sm and Nd isotope ratios. The average value of the two blank solution analyses was used for the correction of acid and gas blank contributions and electronic background. Data reduction of Nd-spiked samples followed the double-isotope dilution equation of Boelrijk (1968). Measured $^{143}Nd/^{144}Nd$ ratios were normalized to $^{146}Nd/^{144}Nd = 0.7219$ and those of Sm to $^{147}Sm/^{149}Sm = 0.56081$ using an exponential law. Long-term reproducibility of the JNdi-1 reference material yielded a $^{143}Nd/^{144}Nd$ of 0.512092 ± 0.000006 (2σ based on 55 measurements over >40 months). Independent, spiked measurements of the GSJ reference material JB-2 gave a long-term reproducibility of $^{143}Nd/^{144}Nd$ and $^{147}Sm/^{144}Nd$ of 0.513080 ± 0.000008 and 0.2145 ± 0.0002, respectively (2σ based on 8 determinations over 12 months), which we used as a conservative measure for the overall uncertainty of the analytical setup. In all but one case, the error estimate of individual measurements of samples ($2\sigma m = 2\sigma/\sqrt{N}$; N = number of scans based on 100 scans per sample, see above) was smaller than the long-term reproducibility of JB-2 measurements. Total procedural blanks of ≤50 pg for Nd and Sm were not significant for the processed element quantities.

3.2. W Isotope Analysis

The W isotopic compositions of samples and reference materials were determined on a ThermoFisher Scientific Neptune Plus MC-ICP-MS at the University of Göttingen. The laboratory and measurement procedures are described in detail in Messling, Wörner, and Willbold (2023). In short, two to six g of sample powder were processed in 60–90 mL PFA beakers. For every 2 g of sample powder, 10 mL 6 M HCl and 10 mL 24 M HF were added. The sample powders were digested at 150°C for 48 hr. After drying completely, 10 mL of 0.5 M HCl—1 M HF was added to the samples and heated for 1–2 hr. The samples were transferred into a 50 mL centrifuge tube and then centrifuged for 15 min. The acid supernatant was decanted and stored in a new centrifuge tube. 10 mL of 0.5 M HCl—1 M HF were added to the fluoride residue, and placed into a heated ultrasonic bath at 60°C for 15 min. After centrifuging and decanting the supernatant, this step was repeated once more. The supernatant of each sample was combined and loaded onto 1 mL anion resin (AG 1x8, 100–200 mesh) and matrix elements were eluted with 0.05 M HCl −1 M HF and 0.5 M HCl −1 vol. % H_2O_2. The W fraction was collected in 3 M HNO_3—0.2 M HF. Subsequently, the W fraction was passed through 1 mL Eichrom prefilter resin to remove any organic compounds. Further separation of high-field strength elements (HFSE) was carried out with 1 mL TEVA resin (Mei et al., 2018) and a 1 mL anion resin column to elute the remaining matrix using 0.05 M HCl −1 M HF. For samples with low W concentrations, several individual digestions (up to 38 g) were combined after the W purification procedure. Typically, 60%–90% of the W budget was recovered using this procedure. The average procedural W blank, following the 6 g sample digestion procedure, was 0.98 ng (n = 13). The relative

blank contribution is below 0.8% for samples with the lowest W concentration and below 1‰ for the average sample and therefore not further considered during data reduction.

The sample solutions are introduced into the MC-ICP-MS using a Teledyne Cetac Aridus III desolvating nebulizer equipped with the Teledyne Cetac QuickWash3 accessory. For the measurement, Faraday cups connected to 10^{11} Ω amplifiers were used for ^{177}Hf, ^{182}W, ^{183}W, ^{184}W and ^{186}W, whereas ^{188}Os was monitored using a 10^{12} Ω amplifier and ^{178}Hf and ^{180}W using 10^{13} Ω amplifiers. Typical sensitivities for a Ni standard sample cone and X-type skimmer cone and an uptake rate of 60 µL/min nebulizer were 300–350 V/ppm of total W. Triplet analyses were conducted for each sample with 60 cycles and an integration time of 8.39 s per analysis. For samples with high W concentrations six (sextuplet analysis) individual measurements were made. Each individual measurement was bracketed with a 220 ng/g W NIST SRM 3163 solution. Data reduction was carried out offline using a Python script applying exponential law to correct for mass bias, normalizing mass fractionation to $^{186}W/^{184}W = 0.92767$ (Völkening et al., 1991). For a high-precision triplet measurement, ca. 550 ng of W were required. The external reproducibility was calculated by repeated measurements of the in-house reference materials "Granite 232" and basalt "Me21," which were measured at the beginning and the end of every measurement sequence. W isotope ratios are reported as $\mu^{182}W$ which is defined as $(^{182}W/^{184}W_{sample}/^{182}W/^{184}W_{NIST\ 3163} - 1) \times 1{,}000{,}000$. The external $\mu^{182}W$ reproducibility (2SD) for Granite 232 is 3.6 ppm ($n = 15$) and 4.3 ppm for basalt Me21 ($n = 24$) for triplet measurements. For sextuplet analysis, the reproducibility was improved to 2.9 ppm for basalt Me21 ($n = 8$).

4. Results

4.1. Sandspruit and Theespruit Formations

The MgO concentrations of the mafic to ultramafic rocks range from 4.7 to 27.9 wt. % and SiO_2 concentrations from 42.7 to 53.7 wt. %, with Al_2O_3/TiO_2 ratios of 5.2–26.6. In primitive upper mantle-normalized trace element plots (Figure 2a), the mafic to ultramafic samples show a continuous range from depletion ($La_N/Yb_N < 1$) to enrichment ($La_N/Yb_N > 2$) of light rare earth elements (LREE), consistent with previously reported data by Jahn et al. (1982) and Schneider et al. (2019) (Figure 2a). LREE-enriched mafic samples have negative Zr and Hf anomalies with Zr/Zr* from 0.7 to 0.8 ($Zr/Zr^* = Zr_N/(Nd_N \times Sm_N)^{0.5}$). The depletion of Zr and Hf is not an effect derived from the incomplete digestion of refractory phases, since Zr and Hf concentrations from low-temperature hot plate digestions are consistent with high-temperature bomb digestions (Data set S1 in Supporting Information S1). The majority of mafic and ultramafic samples are highly enriched in W with W/Th values up to 12.3, roughly 65 times higher than the magmatic W/Th range of 0.07–0.26 (König et al., 2011; Tusch et al., 2021). The ratios are in good agreement with those for komatiite samples from the SGR (Puchtel et al., 2016). Magmatic W/Th ratios were found only for a single sample from the Theespruit Formation (AT 9, W/Th = 0.18). Age-corrected εNd(i) values were normalized to CHUR values of Jacobsen and Wasserburg (1980) with an age of 3.53 Ga based on zircon U-Pb ages of Theespruit volcanic rocks (Kröner et al., 1996; van Kranendonk et al., 2009). Whole rock isochron ages for mafic samples measured in this study give an age of 3.51 ± 0.1 Ga, in good agreement with published zircon ages (Figure S1a in Supporting Information S1). The initial $\varepsilon Nd_{(i)}$ values for the mafic samples range from +0.2 to +2.2 and are in good agreement with the data reported by Jahn et al. (1982) and Schneider et al. (2019). However, in contrast to Schneider et al. (2019), our data do not show a systematic relationship between $\varepsilon Nd_{(i)}$ and the degree of enrichment or depletion of incompatible elements.

The felsic volcanic rocks of the Theespruit Formation have SiO_2 concentrations of 70.2–81.3 wt. %. They show a wide range of K_2O and Na_2O concentrations from 1.7 to 12.5 wt. % and 0.1 to 4.5 wt. %, respectively. Notably, the samples with high CaO (0.1–4.5 wt. %) also have high loss on ignition values (LOI, 0.6–4.8 wt. %). Despite the large variations in the abundances of the alkali metals, their primitive upper mantle-normalized trace element patterns are rather uniform (Figure 2b). Large relative depletion in Sr and Eu reflect preferential partitioning of Sr and Eu into fractionating plagioclase (Agangi et al., 2018; Weill & Drake, 1973). Furthermore, depletion of the high field strength elements (HFSE) Nb, Ta, Ti, Mo, and W (W/Th = 0.016–0.11, Figure 2b) can be observed. In a previous study, Agangi et al. (2018) noted covariations between the HFSE and K_2O abundances in the felsic volcanic rocks. This trend is also well-developed in our data set. Low Nb/La and W/Th ratios are linked with low K_2O and TiO_2 concentrations (Figures 3a, 3b, and 3d) The felsic volcanic rocks have a small range in $\varepsilon Nd_{(i)}$ from −1.0 to +0.2, and agree well with previously published data (Kröner et al., 2013; van Kranendonk et al., 2009). An isochron age of 3.64 ± 0.05 Ga is obtained when combining both mafic and felsic volcanic samples, in agreement with whole rock Nd isotope ages for volcanic rocks from the Sandspruit and Theespruit Formations from Schneider et al. (2019) (Figure S2b in Supporting Information S1).

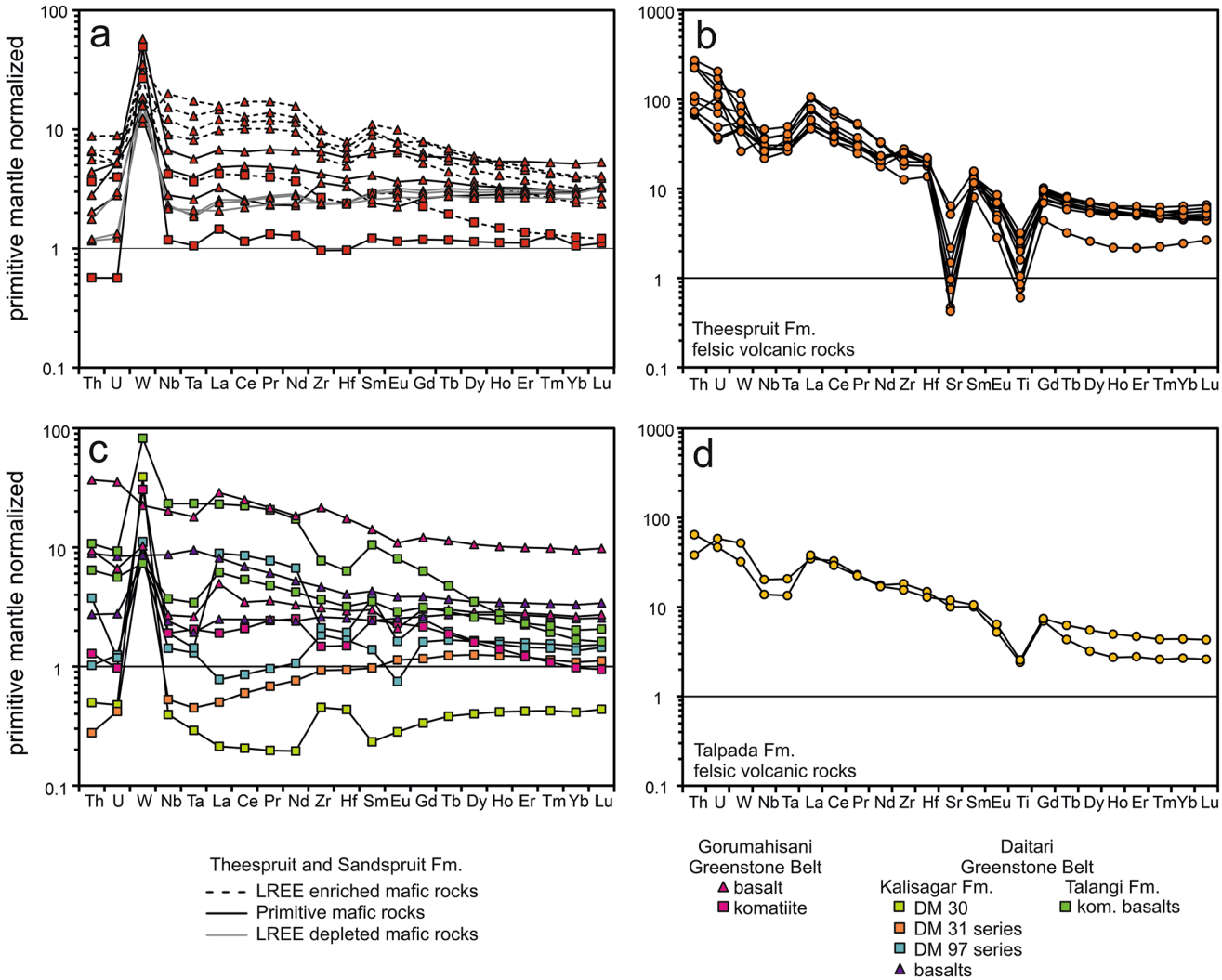

Figure 2. Normalized trace element patterns of mafic and felsic samples from the lower Onverwacht Group and the Badampahar Group. Sample concentrations are normalized to primitive mantle values (Palme & O'Neill, 2014). (a) Mafic samples from the Sandspruit and Theespruit formations. (b) Felsic volcanic rocks from the Theespruit Formation. (c) Representative mafic samples from the Badampahar Group. (d) Felsic volcanic rocks from the Talpada Formation. Felsic rocks are marked with circles, mafic samples with triangles and ultramafic samples with squares.

The W isotopic compositions of felsic and mafic rocks from the Sandspruit and Theespruit formations are shown in Figure 4a. The mafic rocks have $\mu^{182}W$ ranging from $+0.6 \pm 2.9$ to -8.1 ± 4.3. The isotopic compositions of the mafic metavolcanic rocks overlap with the data for the Sandspruit and Theespruit formations published by Tusch et al. (2022) ($\mu^{182}W = +0.8 \pm 3.3$ to -3.2 ± 2.8) but extend to more negative values, coinciding with $\mu^{182}W$ values reported for komatiites of the SGR (Puchtel et al., 2016). The felsic samples from the Theespruit Formation have more uniform W isotope compositions compared to the mafic samples ($\mu^{182}W = +0.3 \pm 4.3$ to -4.7 ± 2.9), with only a single sample exhibiting a resolvable isotope anomaly (Figure 4a). The tonalite samples from the Steynsdorp and Theespruit Pluton have $\mu^{182}W$ values of -4.6 ± 4.3 and -4.5 ± 4.3. The W isotope deficit of the Steynsdorp sample is not as large as the previously reported value of -9.2 ± 2.8 (Tusch et al., 2022); however, both values overlap within error.

4.2. Badampahar Group

The major- and trace element compositions of samples from the Daitari Greenstone Belt have been previously reported in Jodder (2021). In mafic samples, MgO concentrations range from 3.2 to 36.9 wt.%. In the Kalisagar Formation basalts have primitive to enriched LREE patterns (La_N/Yb_N = 1.1–7.4). Contrary to data from

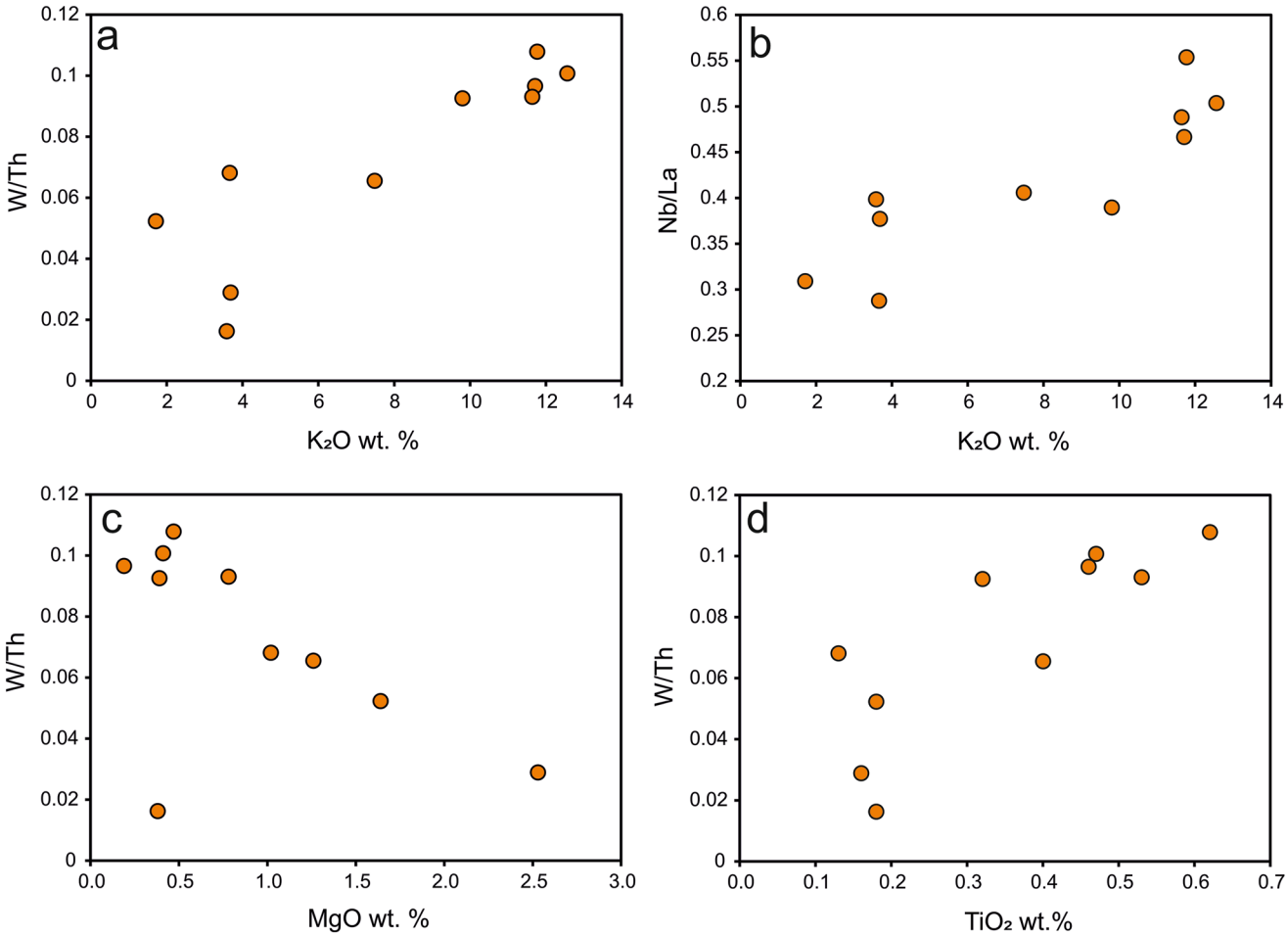

Figure 3. Major element concentrations and trace element ratio diagrams for felsic volcanic rocks from the Theespruit Formation. (a) W/Th against K_2O, (b) Nb/La against K_2O, (c) W/Th against MgO and (d) W/Th against TiO_2.

tabletop digestions reported in Jodder (2021), data for bomb digestions in this study have no depletion in Zr and Hf (Zr/Zr* = 0.9–1.3, Figure S2 in Supporting Information S1). The Zr and Hf disparity between high- and low-temperature digestions indicates the presence of refractory mineral phases such as zircon in the basalts (Blichert-Toft et al., 2004). They further show strong-to-moderate depletion in Nb and Ta (Figure 2c, $Nb_N/La_N = 0.5–1$). Samples from two komatiite flows were collected from the Kalisagar Formation (Jodder, 2021). The lowermost flow (DM 97 A-C) features spinifex komatiites with 22.1–23.8 wt. % MgO. They can be categorized as Al-depleted komatiites ($Al_2O_3/TiO_2 = 11.4$) and have highly variable LREE systematics ($La_N/Yb_N = 0.5–6.5$) with negative Eu anomalies (Eu/Eu* = 0.5 to 0.53). Among the komatiite samples, concentrations of Nb, Ta and Zr, Hf range from strongly depleted to enriched (Figure 2c, Zr/Zr* = 0.4–1.5, $Nb_N/La_N = 0.2–1.8$). Komatiites from the upper komatiite flow (DM 31 A-E) have higher MgO concentrations (22.8–31.5 wt. % MgO) and can be classified as Al-undepleted ($Al_2O_3/TiO_2 = 19.6–22.4$). They have uniform depletion in LREE ($La_N/Yb_N = 0.43–0.56$) and lack any depletion or enrichment of HFSE (Figure 2c). Basalts from the Gorumahisani Greenstone Belt share trace element characteristics with basalts from the Daitari Greenstone Belt (Figure 2c). Komatiites have an MgO concentration of 28.5 wt. % and are depleted in Al ($Al_2O_3/TiO_2 = 6.6$). They are enriched in LREE ($La_N/Yb_N = 1.8–3.8$) and uniformly depleted in Zr and Hf (Zr/Zr* = 0.54 to 0.59). Distinct enrichment in W are present in most mantle-derived mafic rocks of the Badampahar Group (W/Th = 0.09 to 36), while they are not present in the felsic volcanic rocks of the Talpada Formation (W/Th = 0.07–0.19). Although only two samples were measured, the felsic rocks of the Talpada Formation share similar trace element characteristics with the felsic volcanic rocks previously analyzed from the Badampahar Group (Adhikari et al., 2021; Jodder et al., 2021). However, they lack pronounced depletion in Sr (Figure 2d).

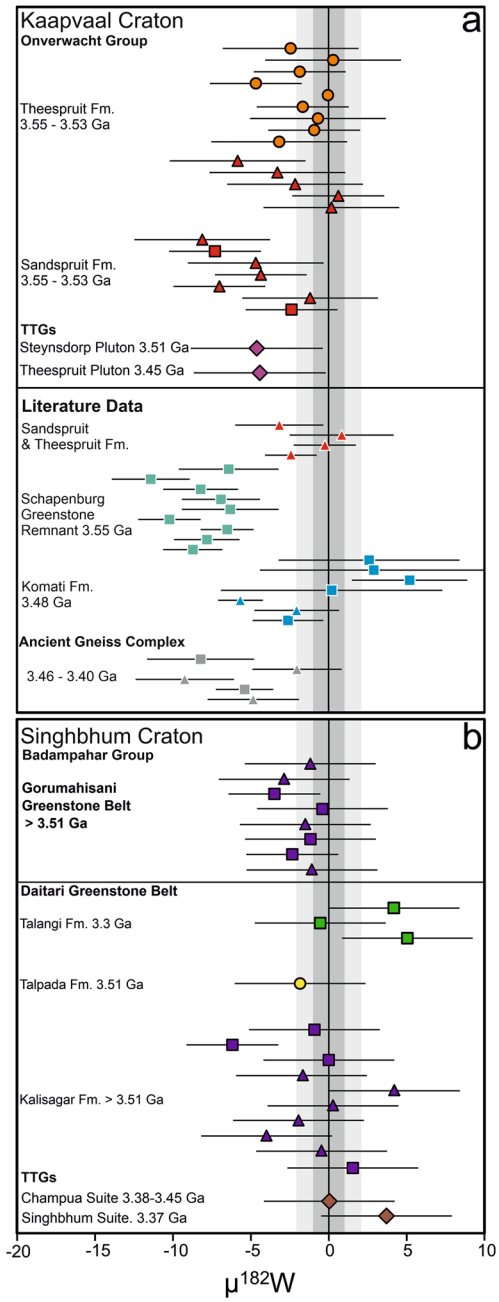

Figure 4. $\mu^{182}W$ values of mafic and felsic samples of the (a) Kaapvaal—and (b) Singhbhum cratons. Circles represent felsic, triangle basaltic and square ultramafic samples. The dark and light gray vertical bars represent the 95% CI and the external reproducibility (2SD) of the in-house reference materials respectively. Literature data from Puchtel et al. (2016), Touboul et al. (2012), and Tusch et al. (2022).

For the samples from the Daitari Greenstone Belt, $\mu^{182}W$ values range from -6.2 ± 2.9 to $+4.2 \pm 4.3$ in the mafic rocks from the >3.51 Ga old Kalisagar Formation, while komatiitic basalts of the younger 3.3 Ga old Talangi Formation exhibit $\mu^{182}W$ between -0.5 ± 4.3 and $+5.1 \pm 4.3$ (Figure 4b). For samples from the Gorumahisani Greenstone Belt, $\mu^{182}W$ values range from -3.5 ± 2.9 to -0.4 ± 4.3 (Figure 4b). Throughout the Badampahar Group, only komatiite sample DM 31 shows a clearly resolvable $\mu^{182}W$ anomaly (DM 31: $\mu^{182}W = -6.2 \pm 2.9$). In contrast, no $\mu^{182}W$ variations are resolvable in samples DM 31B and DM 31D ($\mu^{182}W = -1.7 \pm 4.3$, -0.0 ± 4.3 respectively), although they were sampled from the same komatiite flow. Archean mantle-derived rocks with negative $\mu^{182}W$ variations have so far only been reported in the Kaapvaal Craton (Mundl et al., 2018; Puchtel et al., 2016; Tusch et al., 2022). The Singhbhum Craton is therefore the second Archean craton where this unique isotopic feature is recorded.

5. Discussion

5.1. The Tungsten Budget of Volcanic Rocks From the Kaapvaal and Singhbhum Cratons

The geochemical behavior of W during magmatic processes depends on a variety of factors. Under reducing conditions, W behaves as a moderately siderophile element. Under oxidizing mantle conditions, it is a lithophile element and is considered to be incompatible during mantle melting, similar to Th and U (König et al., 2008; Newsom et al., 1996). Although the W concentration of the mantle and its incompatible nature are still debated (e.g., Peters et al., 2023), all modern Mid Ocean Ridge Basalts (MORB) and Ocean Island Basalts (OIB) show a narrow range of W/Th ratios between 0.07 and 0.26 (Arevalo & McDonough, 2008; Jenner & O'Neill, 2012; König et al., 2011; Kurzweil et al., 2019). MORB-like W/Th values are, however, rarely found in Archean mafic and ultramafic rocks. Most Archean mafic to ultramafic rocks have elevated W/Th ratios, a finding which has been attributed to the fluid-mobile behavior of W and its enrichment during late-stage metamorphism or seafloor alteration (Reifenröther et al., 2021; Reimink et al., 2020; Rizo et al., 2016; Tusch et al., 2019). Figure 5 shows compiled W/Th ratios for a variety of magmatic rocks from the lower Onverwacht and the Badampahar groups. Komatiites from the Onverwacht Group with MgO > 18 wt. % as well as basalts with MgO of 5–12 wt.% typically have W/Th ratios of 0.2–13, which are mostly elevated compared to the mantle range. Samples with intermediate MgO concentrations (i.e., MgO 12–18 wt. %) are not abundant among the analyzed samples but more frequently have MORB-like W/Th ratios than their low- and high-MgO counterparts (Figure 5a). Among the samples from the Kaapvaal Craton, the highest W/Th ratios can be found in the SGR with W/Th ratios of 10–13, which are up to 100 times higher than typical upper mantle values (Puchtel et al., 2016). In this context, it is noteworthy that W/Th ratios have been reported for a total of 100 mafic to ultramafic volcanic rocks from the lower Onverwacht Group (Figure 5a). Critically, despite this significant number, only a single sample with a complimentary W/Th ratio lower than the MORB-like range has been reported. As such, it seems evident that an external source of W is required to explain the ubiquitous enrichment in W concentrations in the mafic volcanic rocks rather than localized redistribution. Conversely, only samples with MORB-like W/Th may preserve the W isotope composition of their original magmatic source. Within the $\mu^{182}W$ data set from the Kaapvaal Craton, only four samples exhibit MORB-like W/Th ratios (Tusch et al., 2022; this study). None of these samples show clearly resolvable W isotope anomalies (average $\mu^{182}W = -2.2 \pm 2.4$), indicating that negative $\mu^{182}W$ values are not intrinsic to the magmatic sources of analyzed volcanic rocks of the

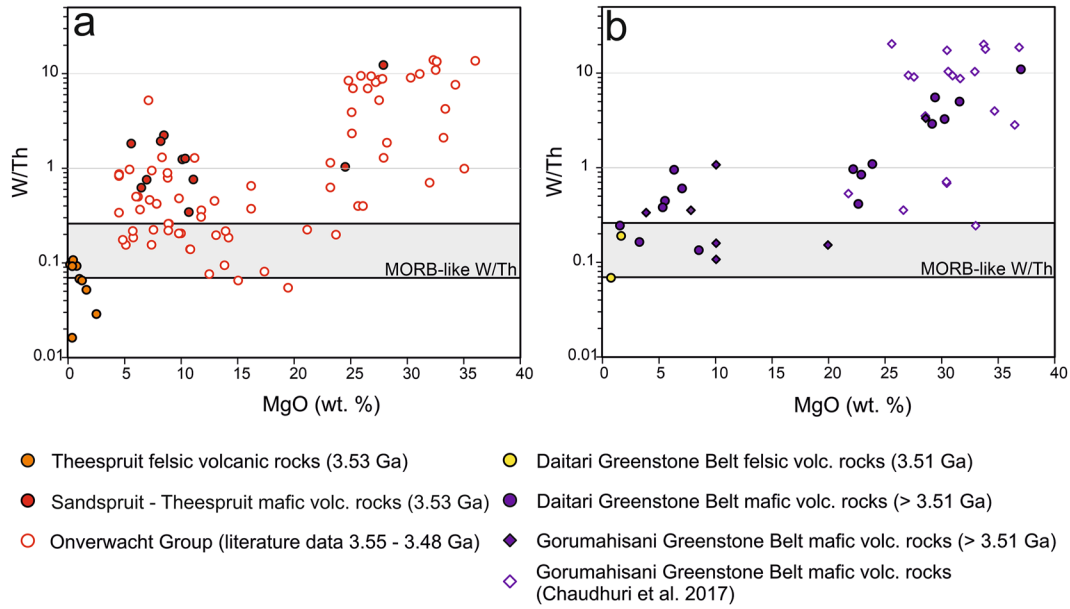

Figure 5. Compiled W/Th ratios and MgO concentrations for samples from (a) the lower Onverwacht Group and (b) the Badampahar Group. Literature data from Chaudhuri et al. (2017), Puchtel et al. (2016), Schneider et al. (2018, 2019), and Tusch et al. (2022). MORB-like W/Th range from Tusch et al. (2021) ranges from 0.07 to 0.26.

Craton. Samples from the Badampahar Group show a similar MgO—W/Th relationship with W/Th ratios up to 20 (Figure 5b). Two samples with MORB-like W/Th ratio have an average $\mu^{182}W$ of -1.3 ± 3.1, supporting mantle sources with modern convecting upper mantle $\mu^{182}W$ values.

Contrasting the data of mafic and ultramafic samples, the felsic volcanic rocks from the Theespruit Formation as well as the Talpada Formation exhibit MORB-like or depleted W/Th ratios, indicating that the fluid-mediated W enrichment only exerts minor control over their W budget. In the Theespruit Formation, however, W/Th ratios show positive correlations with K_2O concentrations and negative correlations with MgO (Figures 3a and 3c). The large increase in K_2O and a concomitant decrease in MgO are commonly associated with K-metasomatism during metamorphic events (e.g., Hofmann & Harris, 2008; Páez et al., 2010). However, fluid immobile HFSEs like Nb and Ti also correlate with K_2O or W/Th ratios (Figures 3b and 3d). Although an increase in W concentrations in felsic volcanic rocks through K-metasomatism has been previously reported (Páez et al., 2010), the influence on Nb and Ti concentrations is usually more limited. It is therefore not clear if the variations in W concentrations are established through K-metasomatism or primary magmatic processes. However, it is worth pointing out that even in samples with MORB-like or depleted W/Th ratios, the W concentrations may have been increased through hydrothermal alteration or low-grade metamorphism. The average W isotopic compositions of felsic volcanic rocks from the Theespruit Formation ($\mu^{182}W = -1.1 \pm 2.2$) and the Talpada Formation ($\mu^{182}W = -1.8 \pm 4.3$). Their W isotope composition are in good agreement with those of mafic volcanic rocks with MORB-like W/Th ratios. The magmatic sources of volcanic rocks from the Kaapvaal and Singhbhum Craton have a W isotope composition similar to the modern mantle, implying the absence of Hadean mantle remnants with an anomalous W isotope composition.

5.2. Mineralogical Controls on the Incorporation of W in Altered Volcanic Rocks

The negative $\mu^{182}W$ values in mafic and ultramafic rocks in the Kaapvaal Craton are restricted to samples enriched in W (W/Th > 0.26). As discussed previously, an external fluid source is required to explain the enrichment in W concentrations of the volcanic rocks and concomitantly their W isotope composition. In magmatic olivine and pyroxene, W is incompatible, resulting in low W concentrations in ultramafic rocks (Arevalo & McDonough, 2008; Liu et al., 2018). By nature, ultramafic rocks are thus more prone to the relative enrichment of incompatible fluid-mobile elements during rock alteration than more evolved rocks with higher incompatible element abundances (e.g., Lahaye & Arndt, 1996). As a consequence, the alteration of volcanic rocks by a W-rich

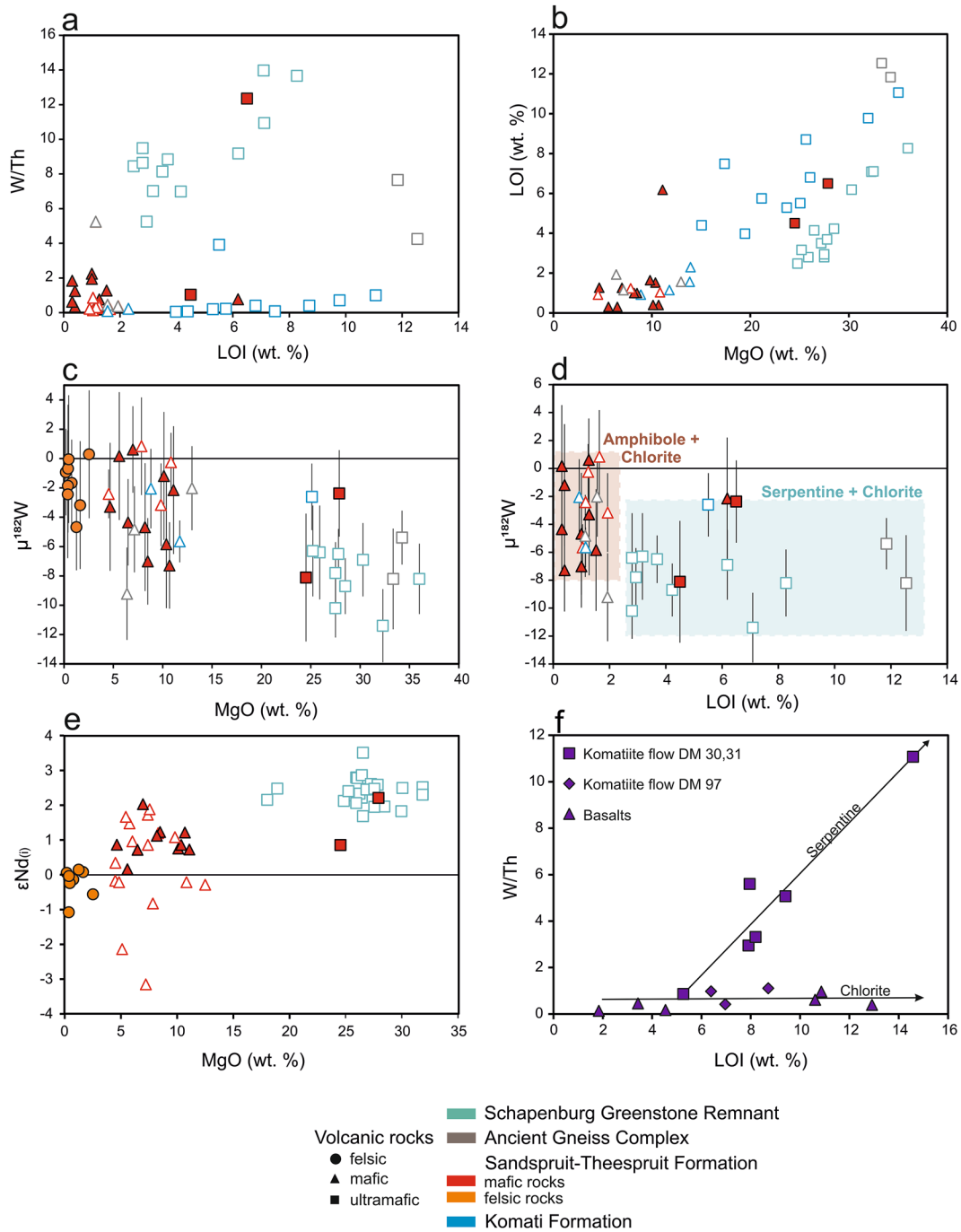

Figure 6. Covariation diagrams for selected geochemical data of samples from the Kaavaal Craton and the Singhbhum Craton. (a–e) Compiled MgO, $\mu^{182}W$, LOI, W/Th, and $\varepsilon Nd_{(i)}$ data from the Onverwacht Group and the Ancient Gneiss Complex. Open symbols are literature data from Puchtel et al. (2016), Tusch et al. (2022), and Schneider et al. (2019). (f) Mafic volcanic rocks from the Kalisagar Formation. Chlorite and serpentine trends represent the dominant hydrous mineral phases determined by XRD analysis.

fluid with a negative $\mu^{182}W$ composition would disproportionately affect ultramafic rocks. As such, the largest $\mu^{182}W$ deficits are generally found in ultramafic samples, while felsic rocks mostly do not exhibit resolvable W isotope anomalies (Figure 6c). Moreover, Figure 6c shows a significant scatter in the W isotope composition of metabasalts. This is likely because they represent chemically diverse source compositions, resulting in a variable susceptibility to secondary W enrichment. Metabasalts, enriched in incompatible trace elements (LREE enriched

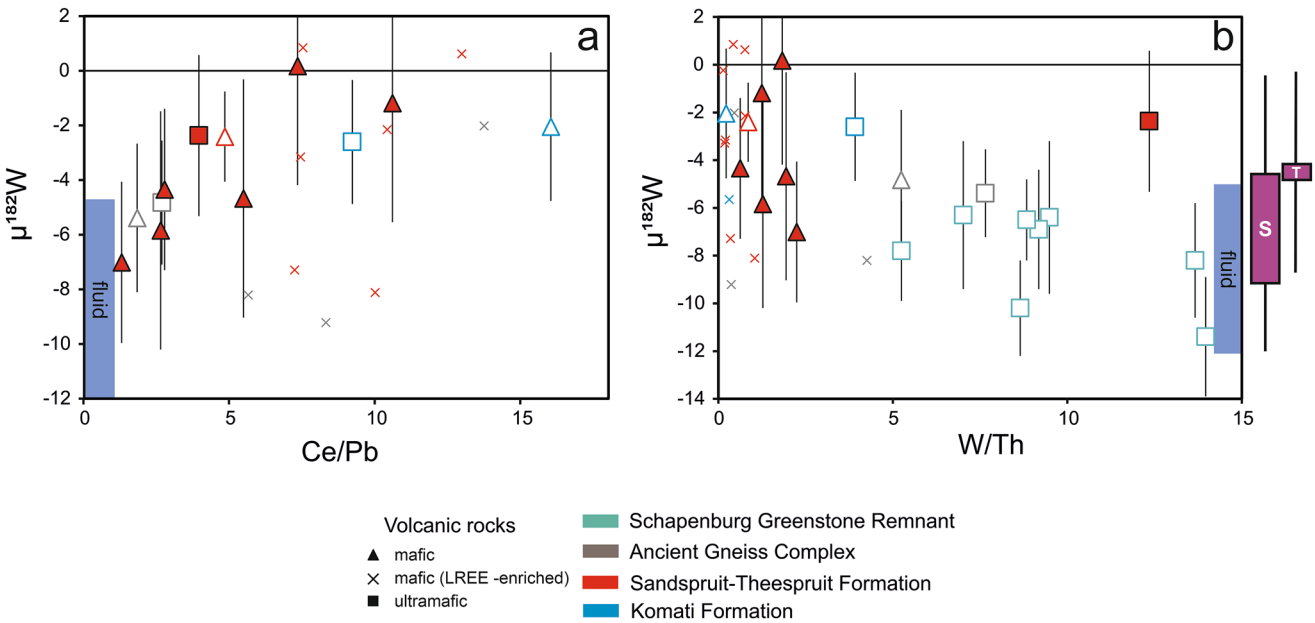

Figure 7. Covariation diagrams between $\mu^{182}W$ and (a) Ce/Pb and (b) W/Th. The data set is filtered for samples with primitive to slightly depleted LREE patterns ($La_N/Yb_N < 2$). The composition of the fluid is constrained by samples with the most negative $\mu^{182}W$ composition. The isotopic composition of the Steynsdorp and Theespruit plutons is indicated by the purple boxes labeled with S and T respectively. Literature data from Puchtel et al. (2016) and Tusch et al. (2022) are shown as open symbols.

group), for example, are also naturally enriched in W (Figure 2c). As a result they are far less susceptible to secondary W enrichment processes than non-enriched (primitive MORB-like) mafic rocks (Figure 2c). Consequently, W/Th ratios of LREE enriched basalts (W/Th = 0.77) are on average 10 times lower than primitive MORB-like mafic rocks (W/Th = 7.66). To better characterize the influence of secondary fluid-induced W enrichment on the mafic and ultramafic volcanic rocks, we filtered the $\mu^{182}W$ data set for samples with primitive to slightly depleted incompatible trace element patterns. These samples should represent the volcanic rocks most susceptible to secondary W enrichment. For the filtered data set, the $\mu^{182}W$ data exhibit covariations with ratios of fluid mobile elements such as Ce/Pb and W/Th (Figure 7). This relationship further indicates that the negative $\mu^{182}W$ values are not an intrinsic magmatic signature, but rather established through an external fluid source. Samples with high W/Th and low Ce/Pb ratios best represent the W isotopic composition of the fluid source. The latter therefore must have had a ^{182}W deficit as low as −12 ppm.

The variable source enrichment of volcanic rocks from the Onverwacht Group certainly has an influence on the relative W enrichment following hydrous alteration. However, another process is required to explain the high W concentrations of ultramafic rocks. This is because the absolute W concentrations of komatiites are higher than those of basalts (komatiites < 1.1 μg/g, basalts < 0.7 μg/g). The difference in concentration is likely caused by differences in the secondary mineral assemblages between both rock types. Fluid-rock interaction typically causes the recrystallization of magmatic, anhydrous minerals to hydrous mineral assemblages like serpentine-group minerals and other phyllosilicates (biotite, phlogopite, and chlorite) (Evans et al., 2013). Hydrous minerals are the main host of W in altered volcanic rocks (Liu et al., 2016, 2018) and become increasingly abundant with increasing MgO in the samples and degree of alteration, as indicated by the increase in LOI (Figure 6b). X-ray diffractometry analysis shows that the ultramafic samples from the Sandspruit Formation contain abundant chlorite, actinolite and antigorite (Table S1 in Supporting Information S1). In the SGR, similar mineralogical assemblages have been reported. Here, komatiites typically comprise 25–70 wt. % serpentine, 20–60 wt. % amphibole and 4–12 wt. % chlorite and magnetite (Lécuyer et al., 1994). Metabasalts, on the other hand, mainly consist of amphibole with serpentine minerals being entirely absent (Table S1 in Supporting Information S1). The komatiite flows of the Kalisagar Formation in the Badampahar Group are variably enriched in W. For komatiite samples DM 30 and DM 31A-E (23–37 wt. % MgO) the W/Th ratios correlate with LOI (Figure 6f). The mineral assemblage of these komatiites comprises serpentine, which is not present in komatiites of the DM 97 series (22–24 wt. % MgO; Table S1 in Supporting Information S1). In the latter, W/Th ratios do not increase with an increasing degree of hydration (LOI), which is also the case for

chlorite-rich basalts from the same formation (Figure 6f). While the altered mafic rocks generally have elevated W/Th ratios exceeding mantle values, W/Th ratios >2 are found only in samples with abundant serpentine, similar to the ultramafic rocks from the Sandspruit Formation and the SGR. The increasing abundance of serpentine with increasing MgO can therefore well explain the correlation between MgO concentrations and W/Th ratios in the samples from the Onverwacht and Badampahar groups (Figure 5). The large abundance of serpentine minerals in komatiites results in an L-shaped pattern in μ^{182}W versus LOI diagram (Figure 6d). While the samples composed primarily of serpentine (i.e., high LOI) show W isotopic compositions entirely dominated by the fluid composition, the effect of these fluids on the W isotopic compositions of metabasalts is much more varied (Figure 6d).

5.3. Origin of W-Rich Fluids in the Kaapvaal Craton

The data support the hypothesis that the mafic and ultramafic volcanic rocks inherited negative μ^{182}W signatures via a fluid-mediated alteration process. As discussed previously, a source with a μ^{182}W composition as low as −12 is required to explain the W isotope composition of the most altered volcanic rocks (high W/Th low Ce/Pb, Figure 7). The initial serpentinization of ultramafic volcanic units likely occurred during seafloor alteration after their emplacement (Alt et al., 2013; Macdonald & Fyfe, 1985). However, it is unlikely that the enrichment of W took place during seawater-related processes because the Paleoarchean seawater likely had a positive μ^{182}W composition. This is because the W budget of seawater is ultimately controlled by igneous rocks (Kurzweil et al., 2021) and positive μ^{182}W anomalies are dominant in global Paleoarchean rock data (e.g., Puchtel et al., 2022; Tusch et al., 2021; Willbold et al., 2011). This assumption is confirmed by the isotopic composition of banded iron formations, which show positive μ^{182}W values throughout the Archean (Mundl-Petermeier et al., 2022; Tusch et al., 2021). Fluid-rock interaction involving seawater can therefore not explain the negative μ^{182}W values in the volcanic rocks of the Kaapvaal Craton.

Widespread, volumetrically dominant granitoid intrusions are features for both, the Kaapvaal and Singhbhum cratons. Incompatible trace elements such as W are enriched in felsic magmatic rocks (upper continental crust ca. 1.9 μg/g W; Rudnick & Gao, 2003) relative to the upper mantle (primitive upper mantle ca. 0.012–0.022 μg/g W; König et al., 2011; Peters et al., 2023). Indeed, felsic magmatic rocks have been previously proposed as the dominant source of W in fluid-overprinted Archean rocks (Liu et al., 2016; Rizo et al., 2016; Willbold et al., 2015).

The plutons within the Stolzburg Block, dated at 3.45 Ga, and the Steynsdorp Pluton, dated at 3.51 Ga, present a substantial volume of silicic intrusions within the lower Onverwacht Group and are therefore a likely source of W-rich fluids (Figure 1a). Indeed, the μ^{182}W composition of the Steynsdorp Pluton has been determined to be -4.6 ± 4.3 and -9.2 ± 2.8 based on two distinct samples (this study; Tusch et al., 2022). The younger Theespruit Pluton displays a slightly lower ^{182}W deficit of -4.5 ± 4.3 ppm. Cumulatively, these findings suggest a consistent prevalence of negative ^{182}W anomalies in the earliest stages of plutonism within the BGGT. This trend may extend to coeval plutons throughout the Kaapvaal Craton, as indicated by observed ^{182}W deficits in the 3.44 Ga old Ngwane Gneiss within the Ancient Gneiss Complex ($\mu^{182}W = -5.9 \pm 3.1$; Tusch et al., 2022).

W-rich fluids mobilized in and removed from these intrusions may therefore provide a viable source of W in the intruded mafic volcanic rocks of the Onverwacht Group, as implied by the shared range of W isotopic compositions (Figure 7b). Conversely, the majority of Paleoarchean granitoids of the Kaapvaal Craton retained their W isotopic source characteristics as can be inferred from their low W/Th ratios (average W/Th = 0.042 Mei et al., 2020; Misra et al., 2017; Tusch et al., 2022). The isotopic heterogeneity within and among the plutons would result in heterogeneous fluid compositions, which can further explain the large variability in μ^{182}W inherited by the volcanic rocks of the Onverwacht Group (Figure 7b). Mobilization of W from felsic intrusions possibly occurred during regional metamorphism (Mei et al., 2020; Rizo et al., 2016; Tusch et al., 2019; Willbold et al., 2015), which took place at ca. 3.23 Ga in the BGGT (Anhaeusser, 2010; Dziggel et al., 2005). However, W-rich fluids may also exsolve from ascending water-saturated melt during the crystallization of high-level plutons, such as the Theespruit Pluton (Anhaeusser, 2010; Audétat et al., 2000), due to the high fluid-melt partition coefficients of W in moderately peraluminous granitic magma (Schmidt et al., 2020). Fluid exsolution is an important process in the formation of W ore deposits involving granitic intrusions (Audétat et al., 2000; Hulsbosch et al., 2016; Meinert et al., 2005) and might therefore also explain the W enrichment in volcanic rocks surrounding Archean granitoid intrusions.

If intrusive rocks are the source of W-rich fluids within the BGGT, it is expected that the spatial relationship between the volcanic units and the felsic intrusive plutons exerts a considerable influence on W isotope

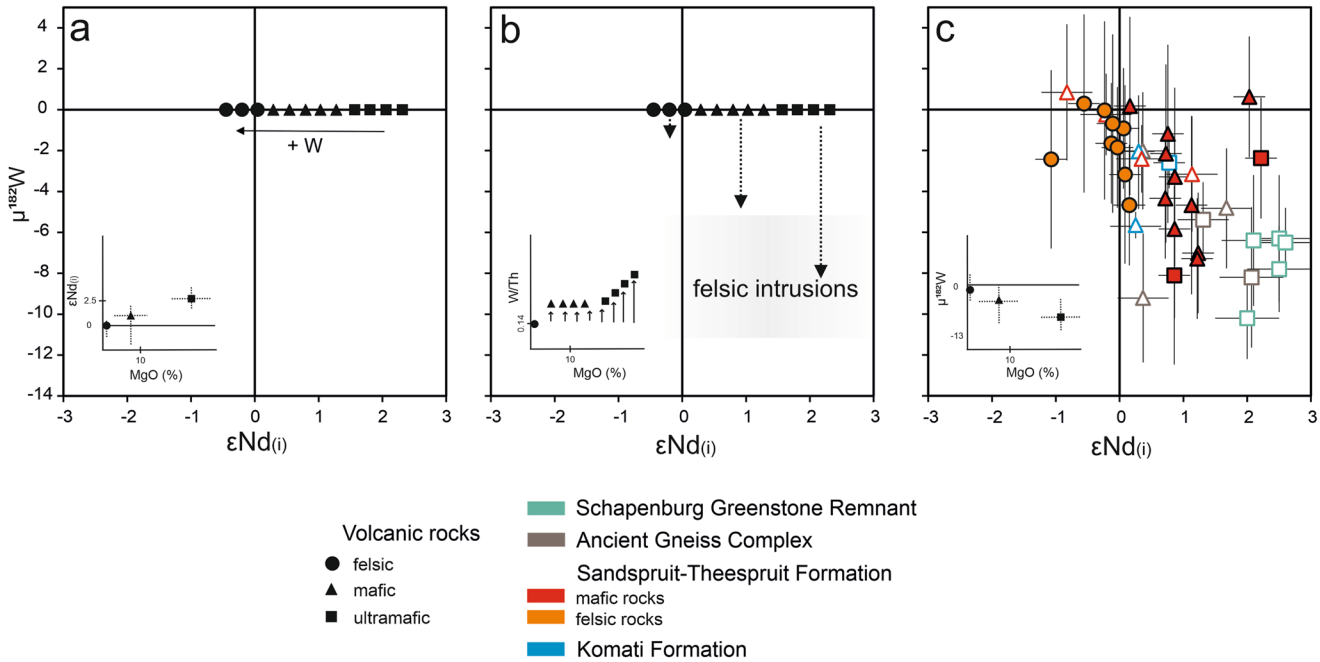

Figure 8. ^{143}Nd and ^{182}W isotopic evolution of the Kaapvaal Craton in three steps. The inset plots in the lower left corner of each panel are the simplified Figures 5a, 6c, and 6e, respectively, and illustrate the major chemical evolution for each step. (a) Initial magmatic isotope composition of volcanic rocks from the Kaapvaal Craton. (b) Changes in the W isotope composition during the fluid-assisted W-mobilization event. The felsic intrusions, marked in gray, are defined by the W isotope composition of the Theespruit and Steynsdorp plutons (this study; Tusch et al., 2022). (c) $\varepsilon Nd_{(i)}$ versus $\mu^{182}W$ data for samples of this study (symbols with black borders) as well as literature data (open symbols) from Puchtel et al. (2016) and Tusch et al. (2022).

systematics in the Onverwacht Group. The largest negative $\mu^{182}W$ values are found in the SGR and the Sandspruit Formation (Figure 4a) that occur as rafts and slivers scattered within the younger granitoid intrusions. Such a close spatial association between plutonic and volcanic rocks is absent in the Komati Formation, at least not at the level of present erosion (Figure 1a). For the Komati Formation, the majority of samples lack any $\mu^{182}W$ deficit, despite the large abundance of serpentinized ultramafic rocks (Figure 4a). Contrary to the SGR, the W/Th ratios in the mafic rocks of the Komati Formation show no increase with increasing LOI (Figure 6b). This behavior suggests that the rocks of the Komati Formation were affected by alteration, albeit the fluid did not contain significant levels of W with a negative $\mu^{182}W$ signature. A possible reason for this could be that the Komati Formation was shielded against granitoid-derived fluids by the stratigraphically underlying older volcanic units of the Onverwacht Group.

5.4. Coupling of $\mu^{182}W$ With $\varepsilon^{143}Nd$ Systematics in the Kaapvaal Craton

Previously, common data trends between the fluid mobile W isotope system and less fluid susceptible $\varepsilon^{143}Nd$ and $\varepsilon^{176}Hf$ data for mafic rocks from the Kaapvaal Craton have been interpreted as primary magmatic W isotope signatures (Tusch et al., 2022). The authors interpreted this trend to represent mixing between two magmatic sources. This interpretation assumed, that the W enrichment derives from an internal redistribution within mafic volcanic units rather than an external source (Puchtel et al., 2016; Tusch et al., 2022). Conversely, this interpretation requires the common occurrence of W-depleted mafic rocks within the same units. However, this is difficult to reconcile with the dominant W enrichment observed in mafic rock samples from the Onverwacht Group (Figure 5a). Combining our new data with those previously published leads to a deterioration in the covariation between $\mu^{182}W$ and $\varepsilon Nd_{(i)}$ data (R^2: Tusch et al., 2022 = 0.47, this study = 0.35, Figure 8c). The slight covariation between both isotope systems does therefore not necessarily represent a mixing process, but may simply reflect a combination of magmatic and alteration processes. We will explore the latter in the following discussion.

Compiled data for volcanic rocks of the Onverwacht Group show that felsic, mafic and ultramafic rocks have distinct $\varepsilon Nd_{(i)}$ isotopic compositions (Figure 6e). The highest $\varepsilon Nd_{(i)}$ values are found in ultramafic samples, while felsic samples have the lowest $\varepsilon Nd_{(i)}$ values. Mafic rocks usually have intermediate $\varepsilon Nd_{(i)}$ values. These

variations can be interpreted as contamination of mafic magma derived from a depleted mantle source by an assimilated, hidden felsic basement (Hoffmann et al., 2020; Schneider et al., 2019). Alternatively, the Nd isotope variation may simply reflect heterogeneous mantle sources of the respective rock types. Regardless of the origin of Nd isotope variations, isotope systems of both W and Nd are broadly linked to the MgO in the studied rocks (Figures 6c and 6e). While this link is of magmatic nature for the Nd isotope system, covariations between MgO and W concentrations can be explained by alteration processes that predominantly affect ultramafic rocks. We can therefore reconcile the W and Nd isotope evolution of the Onverwacht Group in a simple model (Figure 8):

Felsic to ultramafic volcanic rocks with variable $\varepsilon Nd_{(i)}$ are emplaced in the Onverwacht Group from 3.55 to 3.48 Ga. Upon their emplacement, none of the volcanic rocks exhibit any $\mu^{182}W$ variability, consistent with the felsic and least altered mafic rocks found in the Onverwacht Group today (Figure 8a). The volcanic rocks were subsequently altered by either late-stage magmatic fluids during the intrusion of felsic plutons from 3.51 to 3.44 Ga or later by metamorphic fluids at 3.23 Ga during a regional metamorphic event. Regardless of the process, we consider felsic plutons enriched in W as a likely source of $\mu^{182}W$ deficits. The W budget in the serpentine-bearing high $\varepsilon Nd_{(i)}$ komatiites was entirely overprinted by these fluids, while the effect on the low MgO and low $\varepsilon Nd_{(i)}$ altered basalts is more varied (Figure 8b). The felsic volcanic rocks have preserved their primary W isotope composition due to the limited abundance of hydrous minerals and their significant magmatic enrichment in W.

The low variability in $\varepsilon Nd_{(i)}$ values within the different lithological units indicates that this fluid-alteration process does not significantly influence the ^{147}Sm-^{143}Nd isotope systematics. This is supported by the fact that volcanic rocks from the Onverwacht Group plot on the terrestrial $\varepsilon^{176}Hf$—$\varepsilon^{143}Nd$ array (Schneider et al., 2019; Tusch et al., 2022), indicating the pristine nature of both Hf and Nd isotopic tracers. While magmatic processes control long-lived isotope systematics as well as the resulting primary mineral assemblage of a sample, the latter controls the formation of secondary hydrous minerals during alteration. Finally, the secondary mineral assemblage has a major influence on how W is scavenged from fluids and therefore determines the extent of W isotope anomalies.

Further, our findings have implications for the processes that established negative $\mu^{182}W$ values in Hadean mantle reservoirs. Previous studies introduced complex, multistage silicate differentiation models to accommodate positive long-lived Nd isotope values combined with negative short-lived Nd and W isotope systematics within the volcanic rocks of the Kaapvaal Craton (Puchtel et al., 2016; Tusch et al., 2022). According to these studies negative $\mu^{182}W$ variations were established through silicate fractionation based on negative variations in $\mu^{142}Nd$ reported for rocks from the Onverwacht Group (Boyet et al., 2021; Puchtel et al., 2016; Schneider et al., 2018). The short-lived ^{146}Sm—^{142}Nd decay system (half-life of 103 Ma) traces Hadean silicate differentiation similar to the ^{182}Hf- ^{182}W system. In both decay systems, the formation of an enriched reservoir during the Hadean would result in long-term depletion of the daughter isotope. Due to the much longer half-life of the ^{146}Sm -^{142}Nd system, the negative ^{142}Nd signatures may have been established in the Onverwacht mantle source after the extinction of ^{182}Hf. Notably, there is no correlation between $\mu^{182}W$ and $\mu^{142}Nd$ (Tusch et al., 2022), which would be expected if the negative isotopic signatures of both isotopic systems were cogenetic. Core-mantle interaction or an excess of meteoritic material added during Earth's last accretionary phases can also create negative $\mu^{182}W$ values within the mantle (e.g., Archer et al., 2023; Mundl-Petermeier et al., 2020; Touboul et al., 2012). These ideas have been previously precluded based on low concentrations of highly siderophile elements and a modern terrestrial Ru isotope composition of the volcanic rocks (Puchtel et al., 2016; Tusch et al., 2022). However, we have shown that negative $\mu^{182}W$ values, found in the volcanic rocks are completely decoupled from their original magmatic source. Therefore, additional geochemical constraints from altered volcanic units, such as ^{142}Nd data or HSE concentrations, cannot provide any information on the Hadean processes that originally created negative $\mu^{182}W$ values in their fluid source. Conversely, either process, core-mantle interaction, an excess of late accreted material or early differentiation of an enriched silicate reservoir may be viable to explain the origin of negative $\mu^{182}W$ values in the Archean. Further investigations of the chemical composition of BGGT intrusive rocks may reveal the origin of ^{182}W deficits observed in the Kaapvaal Craton in the future.

5.5. Origin of W Enrichment in Volcanic Rocks From the Singhbhum Craton

Although we can identify granitoid-derived fluids as a likely candidate explaining the W enrichment in mafic rocks of the Kaapvaal Craton, the nature of W-rich fluids in the Badampahar Group remains unsolved due to the scarcity of available W isotope data. As previously discussed, the W enrichment factor for the ultramafic samples

of the Badampahar Group is comparable to that of the komatiites from the lower Onverwacht Group (Figures 5a and 5b). A similar source of W-rich fluids is therefore also conceivable for the mafic rocks of the Badampahar Group. A common W enrichment process is plausible, given the similar evolution of both cratons, including the contemporaneous formation of supracrustal greenstone sequences and granitoid intrusions followed by greenschist to amphibolite facies metamorphism (Dziggel et al., 2002; Hofmann et al., 2022; Upadhyay et al., 2014). Contrary to the mafic rocks of the Onverwacht Group, there are no resolvable differences between the W isotopic compositions of the most altered mafic rocks and volcanic rocks with MORB-like W/Th ratios (W/Th > 0.26: $\mu^{182}W = -0.8 \pm 3.9$, W/Th < 0.26: $\mu^{182}W = -0.8 \pm 2.1$). Therefore, we suggest a source of the W-rich fluids with a similar W isotope composition compared to the source of the mafic rocks of the Badampahar Group (i.e., $\mu^{182}W \sim 0$). A single ultramafic sample from a stratified komatiite flow within the Kalisagar Formation exhibits a statistically resolvable negative $\mu^{182}W$ anomaly (i.e., -6.2 ± 2.9), while other samples from the same komatiite flow do not ($\mu^{182}W = -1.7 \pm 4.3$ and 0.0 ± 4.3). This finding implies the existence of granitoids characterized by W isotope deficits within the Singhbhum Craton. A 3.37 Ga old trondhjemitic sill intrusive into the Kalisagar Formation does not exhibit deficits in ^{182}W (DM 77b, $\mu^{182}W = 3.8 \pm 4.3$). Similarly, a gray gneiss sample from the older, 3.38–3.45 Ga old Champua Suite has a non-radiogenic W isotope signature (SB-22, $\mu^{182}W = 0.1 \pm 4.3$). The W isotopic composition of both granitoid suites are in good agreement with the average composition of volcanic rocks within the Badampahar Group, suggesting silicic intrusive rocks as a potential source of W-rich fluids. However, the source of negative $\mu^{182}W$ signatures could not be identified in the Singhbhum Craton, warranting further W isotope investigations of the different phases of felsic plutonism.

6. Conclusions

1. 3.55–3.48 Ga old felsic to ultramafic volcanic rocks from the Singhbhum and Kaapvaal cratons with MORB-like W/Th ratios have $\mu^{182}W$ signatures indistinguishable from the modern upper mantle. Their magmatic sources thus show no evidence for the incorporation of Hadean mantle components.
2. Serpentinized mafic samples from the lower Onverwacht Group are strongly enriched in W. Their overall negative $\mu^{182}W$ values indicate, that fluids derived from spatially associated granitoid intrusions are a likely source of W enrichment. This further implies that the protoliths of 3.5–3.4 Ga old granitoids may be the only Archean magmatic sources characterized by negative $\mu^{182}W$ values to date.
3. Negative W anomalies found in volcanic rocks are decoupled from their original volcanic source. Further geochemical constraints from these rocks cannot be used to differentiate between processes that created negative W anomalies in the Hadean. An excess of late accreted components or core-mantle interaction are therefore viable mechanisms to explain the origin of negative $\mu^{182}W$ values, in addition to the Hadean silicate differentiation, that has been previously proposed.
4. The W isotopic composition of mafic rocks from the Singhbhum Craton indicates that multiple fluid sources are present. The dominant source does not show any resolvable W isotope anomaly. A single komatiite indicates the presence of a source characterized by negative $\mu^{182}W$ values. The Kaapvaal and Singhbhum cratons are therefore the only Archean cratons where negative $\mu^{182}W$ values have been identified so far.
5. The isotopic disparity between volcanic and plutonic rocks of similar age and the interaction between them must be considered when evaluating the origin of their respective sources on a global scale. This relationship is critical in evaluating the W isotopic evolution of the mantle.

Data Availability Statement

All data associated with this study are presented in this paper or are available in Supporting Information S1. Data set S1 is archived in the DIGIS geochemical data repository available at Messling, Jodder, et al. (2023).

Acknowledgments
This study was funded through the priority program 1833 "Building a Habitable Earth" of the German Science Foundation (DFG Grant WI 3579/3-1 to MW). We thank Carl Anhaeusser for organizing the sampling trip to the Sandspruit Formation and Linda Iaccheri for helping with sampling the Theespruit Formation. We acknowledge Dirk Hoffmann for his support with mass spectrometry and clean lab maintenance. We thank Sabrina Metje and Nicole Lockhoff for their assistance with trace element analysis and Leander Kallas for their helpful comments on the manuscript. JJ thanks Odisha Mining Corporation Ltd for their help during fieldwork. We thank Paul Asimow for editorial handling and two anonymous reviewers for their constructive feedback. Open Access funding enabled and organized by Projekt DEAL.

References

Acharyya, S. K., Gupta, A., & Orihashi, Y. (2010). New U-Pb zircon ages from Paleo-Mesoarchean TTG gneisses of the Singhbhum Craton, eastern India. *Geochemical Journal*, *44*(2), 81–88. https://doi.org/10.2343/geochemj.1.0046

Adhikari, A., Mukherjee, S., & Vadlamani, R. (2021). A plume—Mantle interaction model for the petrogenesis of komatiite—Komatiitic basalt—Basalt—basaltic andesite volcanism from the Paleoarchean (3.57–3.31 Ga) Iron Ore Group greenstone belts, Singhbhum Craton, India: Constraints from trace element geochemistry and Sm—Nd geochronology. *Lithos*, *398–399*, 106315. https://doi.org/10.1016/j.lithos.2021.106315

Agangi, A., Hofmann, A., & Elburg, M. A. (2018). A review of Palaeoarchaean felsic volcanism in the eastern Kaapvaal Craton: Linking plutonic and volcanic records. *Geoscience Frontiers*, *9*(3), 667–688. https://doi.org/10.1016/j.gsf.2017.08.003

Alt, J. C., Schwarzenbach, E. M., Früh-Green, G. L., Shanks, W. C., Bernasconi, S. M., Garrido, C. J., et al. (2013). The role of serpentinites in cycling of carbon and sulfur: Seafloor serpentinization and subduction metamorphism. *Lithos*, *178*, 40–54. https://doi.org/10.1016/j.lithos.2012.12.006

Anhaeusser, C. R. (2010). Magmatic and structural characteristics of the ca. 3440 Ma Theespruit Pluton, Barberton mountain land, South Africa. *American Journal of Science*, *310*(9), 1136–1167. https://doi.org/10.2475/09.2010.14

Anhaeusser, C. R. (2014). Archaean greenstone belts and associated granitic rocks—A review. *Journal of African Earth Sciences*, *100*, 684–732. https://doi.org/10.1016/j.jafrearsci.2014.07.019

Archer, G. J., Brennecka, G. A., Gleißner, P., Stracke, A., Becker, H., & Kleine, T. (2019). Lack of late-accreted material as the origin of ^{182}W excesses in the Archean mantle: Evidence from the Pilbara Craton, Western Australia. *Earth and Planetary Science Letters*, *528*, 115841. https://doi.org/10.1016/j.epsl.2019.115841

Archer, G. J., Budde, G., Worsham, E. A., Stracke, A., Jackson, M. G., & Kleine, T. (2023). Origin of ^{182}W anomalies in ocean island basalts. *Geochemistry, Geophysics, Geosystems*, *24*(2), e2022GC010688. https://doi.org/10.1029/2022GC010688

Arevalo, R., & McDonough, W. F. (2008). Tungsten geochemistry and implications for understanding the Earth's interior. *Earth and Planetary Science Letters*, *272*(3–4), 656–665. https://doi.org/10.1016/j.epsl.2008.05.031

Audétat, A., Günther, D., & Heinrich, C. A. (2000). Magmatic-hydrothermal evolution in a fractionating granite: A microchemical study of the Sn-W-F-mineralized mole granite (Australia). *Geochimica et Cosmochimica Acta*, *64*(19), 3373–3393. https://doi.org/10.1016/S0016-7037(00)00428-2

Bali, E., Keppler, H., & Audetat, A. (2012). The mobility of W and Mo in subduction zone fluids and the Mo-W-Th-U systematics of island arc magmas. *Earth and Planetary Science Letters*, *351–352*, 195–207. https://doi.org/10.1016/j.epsl.2012.07.032

Blichert-Toft, J., Arndt, N. T., & Gruau, G. (2004). Hf isotopic measurements on Barberton komatiites: Effects of incomplete sample dissolution and importance for primary and secondary magmatic signatures. *Chemical Geology*, *207*(3–4), 261–275. https://doi.org/10.1016/j.chemgeo.2004.03.005

Boelrijk, N. A. I. M. (1968). A general formula for "double" isotope dilution analysis. *Chemical Geology*, *3*(4), 323–325. https://doi.org/10.1016/0009-2541(68)90037-5

Boyet, M., Garçon, M., Arndt, N., Carlson, R. W., & Konc, Z. (2021). Residual liquid from deep magma ocean crystallization in the source of komatiites from the ICDP drill core in the Barberton Greenstone Belt. *Geochimica et Cosmochimica Acta*, *304*, 141–159. https://doi.org/10.1016/j.gca.2021.04.020

Chaudhuri, T., Satish-Kumar, M., Mazumder, R., & Biswas, S. (2017). Geochemistry and Sm-Nd isotopic characteristics of the Paleoarchean komatiites from Singhbhum Craton, eastern India and their implications. *Precambrian Research*, *298*, 385–402. https://doi.org/10.1016/j.precamres.2017.06.014

Dale, C. W., Kruijer, T. S., & Burton, K. W. (2017). Highly siderophile element and ^{182}W evidence for a partial late veneer in the source of 3.8 Ga rocks from Isua, Greenland. *Earth and Planetary Science Letters*, *458*, 394–404. https://doi.org/10.1016/j.epsl.2016.11.001

de Wit, M. J., Armstrong, R., Hart, R. J., & Wilson, A. H. (1987). Felsic igneous rocks within the 3.3- to 3.5- Ga Barberton Greenstone Belt: High crustal level equivalents of the surrounding Tonalite-Trondhjemite Terrain, emplace during thrusting. *Tectonics*, *6*(5), 529–549. https://doi.org/10.1029/TC006i005p00529

de Wit, M. J., Furnes, H., & Robins, B. (2011). Geology and tectonostratigraphy of the Onverwacht Suite, Barberton Greenstone Belt, South Africa. *Precambrian Research*, *186*(1–4), 1–27. https://doi.org/10.1016/j.precamres.2010.12.007

Dey, S., Topno, A., Liu, Y., & Zong, K. (2017). Generation and evolution of Palaeoarchaean continental crust in the central part of the Singhbhum Craton, eastern India. *Precambrian Research*, *298*, 268–291. https://doi.org/10.1016/j.precamres.2017.06.009

Diener, J. F. A., Stevens, G., Kisters, A. F. M., & Poujol, M. (2005). Metamorphism and exhumation of the basal parts of the Barberton Greenstone Belt, South Africa: Constraining the rates of Mesoarchaean tectonism. *Precambrian Research*, *143*(1–4), 87–112. https://doi.org/10.1016/j.precamres.2005.10.001

Dziggel, A., Armstrong, R. A., Stevens, G., & Nasdala, L. (2005). Growth of zircon and titanite during metamorphism in the granitoid-gneiss terrane south of the Barberton Greenstone Belt, South Africa. *Mineralogical Magazine*, *69*(6), 1019–1036. https://doi.org/10.1180/0026461056960305

Dziggel, A., Stevens, G., Poujol, M., Anhaeusser, C. R., & Armstrong, R. A. (2002). Metamorphism of the granite-greenstone terrane south of the Barberton Greenstone Belt, South Africa: An insight into the tectono-thermal evolution of the "lower" portions of the Onverwacht Group. *Precambrian Research*, *114*(3–4), 221–247. https://doi.org/10.1016/S0301-9268(01)00225-X

Evans, B. W., Hattori, K., & Baronnet, A. (2013). Serpentinite: What, why, where? *Elements*, *9*(2), 99–106. https://doi.org/10.2113/gselements.9.2.99

Grosch, E. G., Kosler, J., McLoughlin, N., Drost, K., Slama, J., & Pedersen, R. B. (2011). Paleoarchean detrital zircon ages from the earliest tectonic basin in the Barberton Greenstone Belt, Kaapvaal Craton, South Africa. *Precambrian Research*, *191*(1–2), 85–99. https://doi.org/10.1016/j.precamres.2011.09.003

Hoffmann, J. E., Musese, E., Kröner, A., Schneider, K. P., Wong, J., Hofmann, A., et al. (2020). Hafnium-Neodymium isotope, trace element and U-Pb zircon age constraints on the petrogenesis of the 3.44–3.46 Ga Dwalile greenstone remnant, Ancient Gneiss Complex, Swaziland. *Precambrian Research*, *351*, 105970. https://doi.org/10.1016/j.precamres.2020.105970

Hofmann, A., & Harris, C. (2008). Silica alteration zones in the Barberton Greenstone Belt: A window into subseafloor processes 3.5-3.3 Ga ago. *Chemical Geology*, *257*(3–4), 221–239. https://doi.org/10.1016/j.chemgeo.2008.09.015

Hofmann, A., Jodder, J., Xie, H., Bolhar, R., Whitehouse, M., & Elburg, M. (2022). The Archaean geological history of the Singhbhum Craton, India—a proposal for a consistent framework of craton evolution. *Earth-Science Reviews*, *228*, 103994. https://doi.org/10.1016/j.earscirev.2022.103994

Hulsbosch, N., Boiron, M. C., Dewaele, S., & Muchez, P. (2016). Fluid fractionation of tungsten during granite-pegmatite differentiation and the metal source of peribatholitic W quartz veins: Evidence from the Karagwe-Ankole Belt (Rwanda). *Geochimica et Cosmochimica Acta*, *175*, 299–318. https://doi.org/10.1016/j.gca.2015.11.020

Jacobsen, S. B., & Wasserburg, G. J. (1980). Sm-Nd isotopic evolution of chondrites. *Earth and Planetary Science Letters*, *50*(1), 139–155. https://doi.org/10.1016/0012-821X(80)90125-9

Jahn, B., Gruau, G., & Glikson, A. Y. (1982). Komatiites of the Onverwacht Group, S. Africa: REE geochemistry, Sm/Nd age and mantle evolution. *Contributions to Mineralogy and Petrology*, *80*(1), 25–40. https://doi.org/10.1007/BF00376732

Jenner, F. E., & O'Neill, H. S. C. (2012). Analysis of 60 elements in 616 ocean floor basaltic glasses. *Geochemistry, Geophysics, Geosystems*, *13*(2), Q02005. https://doi.org/10.1029/2011GC004009

Jodder, J. (2021). The geology of the Daitari Greenstone Belt, Singhbhum Craton, India—Insights into early life 3.5 Ga ago. (Doctoral thesis). University of Johannesburg.

Jodder, J., Hofmann, A., & Ueckermann, H. (2021). 3.51 Ga old felsic volcanic rocks and carbonaceous cherts from the Gorumahisani Greenstone Belt—Insights into the Palaeoarchaean record of the Singhbhum Craton, India. *Precambrian Research*, *357*, 106109. https://doi.org/10.1016/j.precamres.2021.106109

Jodder, J., Hofmann, A., Xie, H., Elburg, M. A., & Wilson, A. (2023). Geochronology of the Daitari Greenstone Belt, Singhbhum Craton, India. *Precambrian Research*, *388*, 106997. https://doi.org/10.1016/j.precamres.2023.106997

König, S., Münker, C., Hohl, S., Paulick, H., Barth, A. R., Lagos, M., et al. (2011). The Earth's tungsten budget during mantle melting and crust formation. *Geochimica et Cosmochimica Acta*, *75*(8), 2119–2136. https://doi.org/10.1016/j.gca.2011.01.031

König, S., Münker, C., Schuth, S., & Garbe-schönberg, D. (2008). Mobility of tungsten in subduction zones. *Earth and Planetary Science Letters*, *274*(1–2), 82–92. https://doi.org/10.1016/j.epsl.2008.07.002

Kröner, A., Anhaeusser, C. R., Hoffmann, J. E., Wong, J., Geng, H., Hegner, E., et al. (2016). Chronology of the oldest supracrustal sequences in the Palaeoarchaean Barberton Greenstone Belt, South Africa and Swaziland. *Precambrian Research*, *279*, 123–143. https://doi.org/10.1016/j.precamres.2016.04.007

Kröner, A., Hegner, E., Wendt, J. I., & Byerly, G. R. (1996). The oldest part of the Barberton granitoid-greenstone terrain, South Africa: Evidence for crust formation between 3.5 and 3.7 Ga. *Precambrian Research*, *78*(1–3), 105–124. https://doi.org/10.1016/0301-9268(95)00072-0

Kröner, A., Hoffmann, J. E., Xie, H., Wu, F., Münker, C., Hegner, E., et al. (2013). Generation of early Archaean felsic greenstone volcanic rocks through crustal melting in the Kaapvaal, craton, southern Africa. *Earth and Planetary Science Letters*, *381*, 188–197. https://doi.org/10.1016/j.epsl.2013.08.029

Kurzweil, F., Archer, C., Wille, M., Schoenberg, R., Münker, C., & Dellwig, O. (2021). Redox control on the tungsten isotope composition of seawater. *Proceedings of the National Academy of Sciences of the United States of America*, *118*(18), e2023544118. https://doi.org/10.1073/pnas.2023544118

Kurzweil, F., Münker, C., Grupp, M., Braukmüller, N., Fechtner, L., Christian, M., et al. (2019). The stable tungsten isotope composition of modern igneous reservoirs. *Geochimica et Cosmochimica Acta*, *251*, 176–191. https://doi.org/10.1016/j.gca.2019.02.025

Lahaye, Y., & Arndt, N. T. (1996). Alteration of a komatiite flow from Alexo, Ontario, Canada. *Journal of Petrology*, *37*(6), 1261–1284. https://doi.org/10.1093/petrology/37.6.1261

Lécuyer, C., Gruau, G., Anhaeusser, C. R., & Fourcade, S. (1994). The origin of fluids and the effects of metamorphism on the primary chemical compositions of Barberton komatiites: New evidence from geochemical (REE) and isotopic (Nd, O, H, $^{39}Ar/^{40}Ar$) data. *Geochimica et Cosmochimica Acta*, *58*(2), 969–984. https://doi.org/10.1016/0016-7037(94)90519-3

Liu, J., Pearson, D. G., Chacko, T., & Luo, Y. (2018). A reconnaissance view of tungsten reservoirs in some crustal and mantle rocks: Implications for interpreting W isotopic compositions and crust-mantle W cycling. *Geochimica et Cosmochimica Acta*, *223*, 300–318. https://doi.org/10.1016/j.gca.2017.12.015

Liu, J., Touboul, M., Ishikawa, A., Walker, R. J., & Pearson, D. G. (2016). Widespread tungsten isotope anomalies and W mobility in crustal and mantle rocks of the Eoarchean Saglek Block, northern Labrador, Canada: Implications for early Earth processes and W recycling. *Earth and Planetary Science Letters*, *448*, 13–23. https://doi.org/10.1016/j.epsl.2016.05.001

Macdonald, A. H., & Fyfe, W. S. (1985). Rate of serpentinization in seafloor environments. *Tectonophysics*, *116*(1–2), 123–135. https://doi.org/10.1016/0040-1951(85)90225-2

Mei, Q. F., Yang, J. H., Wang, Y. F., Wang, H., & Peng, P. (2020). Tungsten isotopic constraints on homogenization of the Archean silicate Earth: Implications for the transition of tectonic regimes. *Geochimica et Cosmochimica Acta*, *278*, 51–64. https://doi.org/10.1016/j.gca.2019.07.050

Mei, Q. F., Yang, J. H., & Yang, Y. H. (2018). An improved extraction chromatographic purification of tungsten from a silicate matrix for high precision isotopic measurements using MC-ICPMS. *Journal of Analytical Atomic Spectrometry*, *33*(4), 569–577. https://doi.org/10.1039/c8ja00024g

Meinert, L. D., Dipple, G. M., & Nicolescu, S. (2005). World Skarn deposits. In *Economic geology, one hundredth anniversary* (pp. 299–336). https://doi.org/10.5382/av100.11

Messling, N., Jodder, J., Hegner, E., Hofmann, A., Wemmer, K., & Willbold, M. (2023). W isotope, Nd isotope, major and trace element data from the Badampahar and Onverwacht Groups, Kaapvaal and Singhbhum Cratons [Dataset]. GFZ Data Services. https://doi.org/10.5880/digis.2023.005

Messling, N., Wörner, G., & Willbold, M. (2023). Ancient mantle plume components constrained by tungsten isotope variability in arc lavas. *Geochemical Perspectives Letters*, *26*, 31–35. https://doi.org/10.7185/geochemlet.2321

Misra, S., Reinhardt, J., & Wilson, A. H. (2017). Petrochemical evolution of the White Mfolozi Granite pluton: Evidence for a late Palaeoarchaean A-type granite from the SE Kaapvaal Craton, South Africa. *Lithos*, *286–287*, 480–501. https://doi.org/10.1016/j.lithos.2017.05.022

Mitra, A., Dey, S., Das, P., Zong, K., Liu, Y., Mitra, A., & Gond, A. K. (2022). Time-space evolution of an ancient continent, a window to changing crustal architecture: Insights from granitoids of Singhbhum Craton, eastern India. *Earth-Science Reviews*, *234*, 104183. https://doi.org/10.1016/j.earscirev.2022.104183

Moyen, J.-F., Stevens, G., Kisters, A. F. M., Belcher, R. W., & Lemirre, B. (2019). TTG plutons of the Barberton granitoid-greenstone terrain, South Africa. *Earth's Oldest Rocks*, 615–653. https://doi.org/10.1016/b978-0-444-63901-1.00025-3

Mundl, A., Walker, R. J., Reimink, J. R., Rudnick, R. L., & Gaschnig, R. M. (2018). Tungsten-182 in the upper continental crust: Evidence from glacial diamictites. *Chemical Geology*, *494*, 144–152. https://doi.org/10.1016/j.chemgeo.2018.07.036

Mundl-Petermeier, A., Viehmann, S., Tusch, J., Bau, M., Kurzweil, F., & Münker, C. (2022). Earth's geodynamic evolution constrained by ^{182}W in Archean seawater. *Nature Communications*, *13*, 2710. https://doi.org/10.1038/s41467-022-30423-3

Mundl-Petermeier, A., Walker, R. J., Fischer, R. A., Lekic, V., Jackson, M. G., & Kurz, M. D. (2020). Anomalous ^{182}W in high $^{3}He/^{4}He$ ocean island basalts: Fingerprints of Earth's core? *Geochimica et Cosmochimica Acta*, *271*, 194–211. https://doi.org/10.1016/j.gca.2019.12.020

Nakamura, K., & Kato, Y. (2004). Carbonatization of oceanic crust by the seafloor hydrothermal activity and its significance as a CO_2 sink in the Early Archean. *Geochimica et Cosmochimica Acta*, *68*(22), 4595–4618. https://doi.org/10.1016/j.gca.2004.05.023

Nakanishi, N., Puchtel, I. S., Walker, R. J., & Nabelek, P. I. (2023). Dissipation of Tungsten-182 anomalies in the Archean upper mantle: Evidence from the Black Hills, South Dakota, USA. *Chemical Geology*, *617*, 121255. https://doi.org/10.1016/j.chemgeo.2022.121255

Nelson, D. R., Bhattacharya, H. N., Thern, E. R., & Altermann, W. (2014). Geochemical and ion-microprobe U-Pb zircon constraints on the Archaean evolution of Singhbhum Craton, eastern India. *Precambrian Research*, *255*(P1), 412–432. https://doi.org/10.1016/j.precamres.2014.09.024

Newsom, H. E., Sims, K. W. W., Noll, P. D., Jaeger, W. L., Maehr, S. A., & Beserra, T. B. (1996). The depletion of tungsten in the bulk silicate Earth: Constraints on core formation. *Geochimica et Cosmochimica Acta*, *60*(7), 1155–1169. https://doi.org/10.1016/0016-7037(96)00029-4

Olierook, H. K. H., Clark, C., Reddy, S. M., Mazumder, R., Jourdan, F., & Evans, N. J. (2019). Evolution of the Singhbhum Craton and supracrustal provinces from age, isotopic and chemical constraints. *Earth-Science Reviews*, *193*, 237–259. https://doi.org/10.1016/j.earscirev.2019.04.020

Páez, G. N., Ruiz, R., Guido, D. M., Jovic, S. M., & Schalamuk, I. B. (2010). The effects of K-metasomatism in the Bahía Laura Volcanic Complex, Deseado Massif, Argentina: Petrologic and metallogenic consequences. *Chemical Geology*, *273*(3–4), 300–313. https://doi.org/10.1016/j.chemgeo.2010.03.007

Palme, H., & O'Neill, H. S. (2014). Cosmochemical estimates of mantle composition. In *Treatise on Geochemistry* (2nd ed., Vol. 3, pp. 1–39). https://doi.org/10.1016/B978-0-08-095975-7.00201-1

Peters, D., Rizo, H., Carlson, R. W., Walker, R. J., Rudnick, R. L., & Luguet, A. (2023). Tungsten in the mantle constrained by continental lithospheric peridotites: Less incompatible and more abundant. *Geochimica et Cosmochimica Acta*, *351*, 167–180. https://doi.org/10.1016/j.gca.2023.04.016

Puchtel, I. S., Blichert-Toft, J., Horan, M. F., Touboul, M., & Walker, R. J. (2022). The komatiite testimony to ancient mantle heterogeneity. *Chemical Geology*, *594*, 120776. https://doi.org/10.1016/j.chemgeo.2022.120776

Puchtel, I. S., Blichert-Toft, J., Touboul, M., Horan, M. F., & Walker, R. J. (2016). The coupled ^{182}W-^{142}Nd record of early terrestrial mantle differentiation. *Geochemistry, Geophysics, Geosystems*, *17*(6), 2168–2193. https://doi.org/10.1002/2016GC006324

Puchtel, I. S., Walker, R. J., Anhaeusser, C. R., & Gruau, G. (2009). Re-Os isotope systematics and HSE abundances of the 3.5 Ga Schapenburg komatiites, South Africa: Hydrous melting or prolonged survival of primordial heterogeneities in the mantle? *Chemical Geology*, *262*(3–4), 355–369. https://doi.org/10.1016/j.chemgeo.2009.02.006

Reifenröther, R., Münker, C., & Scheibner, B. (2021). Evidence for tungsten mobility during oceanic crust alteration. *Chemical Geology*, *584*, 120504. https://doi.org/10.1016/j.chemgeo.2021.120504

Reimink, J. R., Mundl-Petermeier, A., Carlson, R. W., Shirey, S. B., Walker, R. J., & Pearson, D. G. (2020). Tungsten isotope composition of Archean crustal reservoirs and implications for terrestrial μ^{182}W evolution. *Geochemistry, Geophysics, Geosystems*, *21*(7), e2020GC009155. https://doi.org/10.1029/2020GC009155

Richard, P., Shimizu, N., & Allègre, C. J. (1976). ^{143}Nd/^{146}Nd, a natural tracer: An application to ocean island basalts. *Earth and Planetary Science Letters*, *31*(2), 269–278. https://doi.org/10.1016/0012-821x(76)90219-3

Rizo, H., Walker, R. J., Carlson, R. W., Touboul, M., Horan, M. F., Puchtel, I. S., et al. (2016). Early Earth differentiation investigated through ^{142}Nd, ^{182}W, and highly siderophile element abundances in samples from Isua, Greenland. *Geochimica et Cosmochimica Acta*, *175*, 319–336. https://doi.org/10.1016/j.gca.2015.12.007

Rudnick, R. L., & Gao, S. (2003). Composition of the continental crust. In *The crust* (2nd ed., Vol. 3, pp. 1–51). https://doi.org/10.1016/B978-0-08-095975-7.00301-6

Schmidt, C., Romer, R. L., Wohlgemuth-Ueberwasser, C. C., & Appelt, O. (2020). Partitioning of Sn and W between granitic melt and aqueous fluid. *Ore Geology Reviews*, *117*, 103263. https://doi.org/10.1016/j.oregeorev.2019.103263

Schneider, K. P., Hoffmann, J. E., Boyet, M., Münker, C., & Kröner, A. (2018). Coexistence of enriched and modern-like ^{142}Nd signatures in Archean igneous rocks of the eastern Kaapvaal Craton, southern Africa. *Earth and Planetary Science Letters*, *487*, 54–66. https://doi.org/10.1016/j.epsl.2018.01.022

Schneider, K. P., Hoffmann, J. E., Münker, C., Patyniak, M., Sprung, P., Roerdink, D., et al. (2019). Petrogenetic evolution of metabasalts and metakomatiites of the lower Onverwacht Group, Barberton Greenstone Belt (South Africa). *Chemical Geology*, *511*, 152–177. https://doi.org/10.1016/j.chemgeo.2019.02.020

Shibuya, T., Komiya, T., Nakamura, K., Takai, K., & Maruyama, S. (2010). Highly alkaline, high-temperature hydrothermal fluids in the early Archean ocean. *Precambrian Research*, *182*(3), 230–238. https://doi.org/10.1016/j.precamres.2010.08.011

Touboul, M., Liu, J., O'Neil, J., Puchtel, I. S., & Walker, R. J. (2014). New insights into the Hadean mantle revealed by ^{182}W and highly siderophile element abundances of supracrustal rocks from the Nuvvuagittuq Greenstone Belt, Quebec, Canada. *Chemical Geology*, *383*, 63–75. https://doi.org/10.1016/j.chemgeo.2014.05.030

Touboul, M., Puchtel, I. S., & Walker, R. J. (2012). ^{182}W evidence for long-term preservation of early mantle differentiation products. *Science*, *335*(6072), 1065–1069. https://doi.org/10.1126/science.1216351

Tusch, J., Hoffmann, J. E., Hasenstab, E., Fischer-Gödde, M., Marien, C. S., Wilson, A. H., & Münker, C. (2022). Long-term preservation of Hadean protocrust in Earth's mantle. *Proceedings of the National Academy of Sciences of the United States of America*, *119*(18), e2120241119. https://doi.org/10.1073/pnas.2120241119

Tusch, J., Münker, C., Hasenstab, E., Jansen, M., Marien, C. S., Kurzweil, F., et al. (2021). Convective isolation of Hadean mantle reservoirs through Archean time. *Proceedings of the National Academy of Sciences of the United States of America*, *118*(2), e2012626118. https://doi.org/10.1073/pnas.2012626118

Tusch, J., Sprung, P., van de Löcht, J., Hoffmann, J. E., Boyd, A. J., Rosing, M. T., & Münker, C. (2019). Uniform ^{182}W isotope compositions in Eoarchean rocks from the Isua region, SW Greenland: The role of early silicate differentiation and missing late veneer. *Geochimica et Cosmochimica Acta*, *257*, 284–310. https://doi.org/10.1016/j.gca.2019.05.012

Upadhyay, D., Chattopadhyay, S., Kooijman, E., Mezger, K., & Berndt, J. (2014). Magmatic and metamorphic history of Paleoarchean tonalite-trondhjemite-granodiorite (TTG) suite from the Singhbhum craton, eastern India. *Precambrian Research*, *252*, 180–190. https://doi.org/10.1016/j.precamres.2014.07.011

van Kranendonk, M. J., Kröner, A., Hegner, E., & Connelly, J. (2009). Age, lithology and structural evolution of the c. 3.53 Ga Theespruit Formation in the Tjakastad area, southwestern Barberton Greenstone Belt, South Africa, with implications for Archaean tectonics. *Chemical Geology*, *261*(1–2), 115–139. https://doi.org/10.1016/j.chemgeo.2008.11.006

Viljoen, M. J., & Viljoen, R. P. (1969). An introduction to the geology of the Barberton granite-greenstone terrain. *Geological Society of South Africa Special Publication*, *2*, 928.

Vockenhuber, C., Oberli, F., Bichler, M., Ahmad, I., Quitté, G., Meier, M., et al. (2004). New half-life measurement of ^{182}Hf: Improved chronometer for the early solar system. *Physical Review Letters*, *93*(17), 172501. https://doi.org/10.1103/PhysRevLett.93.172501

Völkening, J., Köppe, M., & Heumann, K. G. (1991). Tungsten isotope ratio determinations by negative thermal ionization mass spectrometry. *International Journal of Mass Spectrometry and Ion Processes*, *107*(2), 361–368. https://doi.org/10.1016/0168-1176(91)80070-4

Weill, D. F., & Drake, M. J. (1973). Europium anomaly in plagioclase feldspar: Experimental results and semiquantitative model. *Science*, *180*(4090), 1059–1060. https://doi.org/10.1126/science.180.4090.1059

Willbold, M., Elliott, T., & Moorbath, S. (2011). The tungsten isotopic composition of the Earth's mantle before the terminal bombardment. *Nature*, *477*(7363), 195–198. https://doi.org/10.1038/nature10399

Willbold, M., Mojzsis, S. J., Chen, H. W., & Elliott, T. (2015). Tungsten isotope composition of the Acasta Gneiss Complex. *Earth and Planetary Science Letters*, *419*, 168–177. https://doi.org/10.1016/j.epsl.2015.02.040

References From the Supporting Information

Hegner, E., Alexeiev, D. V., Messling, N., Tolmacheva, T. Y., & Willbold, M. (2022). Cambrian-Ordovician mid-ocean ridge magmatism in the Kyrgyz Middle Tianshan and origin of the Karaterek ophiolite. *Lithos*, *410–411*, 106576. https://doi.org/10.1016/j.lithos.2021.106576

Vermeesch, P. (2018). IsoplotR: A free and open toolbox for geochronology. *Geoscience Frontiers*, *9*(5), 1479–1493. https://doi.org/10.1016/j.gsf.2018.04.001